Decision Analytics Journal 10 (2024) 100368

Contents lists available at ScienceDirect

Decision Analytics Journal

journal homepage: www.elsevier.com/locate/dajour

A new optimisation framework based on Monte Carlo embedded hybrid variant mean–variance mapping considering uncertainties

Norhafidzah Mohd Saad [a], Muhamad Zahim Sujod [a,*], Mohd Ikhwan Muhammad Ridzuan [a], Mohammad Fadhil Abas [a], Mohd Shawal Jadin [a], Mohd Fadzil Abdul Kadir [b]

[a] Faculty of Electrical & Electronics Engineering Technology, Universiti MalaysiaPahang Al-Sultan Abdullah (UMPSA), 26600 Pekan Pahang, Malaysia
[b] Faculty of Informatics and Computing, Universiti Sultan Zainal Abidin, Kampus Besut, 22200 Besut, Terengganu, Malaysia

ARTICLE INFO

Keywords:
Optimisation
Photovoltaic distributed generation
Power loss minimisation
Probabilistic power flow
Siting and sizing
Uncertainty energy management

ABSTRACT

This study proposes a new optimisation framework based on Monte Carlo embedded hybrid variant mean–variance mapping (MVMO-SH) optimisation for planning Photovoltaic Distributed Generation (PVDG) in the urban Radial Distribution Network (RDN). The Active Power Loss (APL) index was calculated considering the risk of uncertain photovoltaic generation and urban load distributions. The Monte Carlo Probability Density Function method was initially used to manage uncertainties. The Monte Carlo-embedded MVMO-SH was then used to optimise PVDG in the urban RDN. Simulations were run for several scenarios in three load cases based on 288 segments: residential, commercial, and industrial urban loads. The MVMO-SH had the lowest APL index compared to genetic algorithm and particle swarm optimisation when the probabilistic power flow with PVDG was optimised under uncertainty. The APL indexes with three PVDG installations in the 33-bus RDN for residential, commercial, and industrial urban load models were 0.4094, 0.4811, and 0.4655, respectively. In the 69-bus RDN, the APL indexes with three PVDG installations for residential, commercial, and industrial urban load models were 0.3403, 0.3570, and 0.3504, respectively. For all load models examined, there was a significant reduction in the APL index for the case of three PVDGs compared to the system without PVDG. The findings showed that uncertainty significantly impacted the optimal location and size of PVDG in the RDN.

1. Introduction

The availability of solar resources is an unpredictable factor, influenced by several environmental, meteorological, and weather-related aspects. Cloud cover, haze, fog, and rapid temperature changes create uncertainty, leading to instability in energy output from photovoltaic distributed generation (PVDG) [1]. The variation in load patterns poses an additional challenge for the distribution system [2]. As a result, it is crucial to consider these factors while incorporating PVDG into power systems. The use of probabilistic approaches for predicting solar photovoltaic generation and load uncertainties is essential to address the impact of PVDG integration on the power system network. Uncertainties are location-specific and influenced by geographical factors. Therefore, managing and characterising them using historical meteorological data is vital for PVDG optimisation in the power system [3]. Finally, the PVDG rating size depends on the network's load condition, which must be carefully evaluated [4].

Numerous research papers have delved into the optimal location and size of photovoltaic distributed generation (PVDG). However, a majority of them employ deterministic methods. For instance, [5] employs the Manta Ray Foraging optimisation algorithm (MRFO) to identify the most suitable distributed generation type I locations and sizes. Meanwhile, [6] proposes Nature-Inspired optimisation algorithms and compares the results of the Moth Flame Optimisation (MFO) algorithm with two other algorithms, the Grasshopper Optimisation Algorithm (GOA) and Salp Swarm Algorithm (SSA). The study concludes that MFO is more effective in selecting the distributed generation locations and sizes than GOA and SSA.

Other novel methods have also been introduced, such as [7]'s self-organising hierarchical binary particle swarm optimisation for determining optimal PV unit size in RDN and [8]'s severity performance index (SPI) to rank the most critical buses for PVDG allocation. Additionally, [9] developed a weight factor method for optimal reconfiguration of radial distribution systems with solar and wind energy resources. The Moth–Flame Optimisation algorithm was used to determine the best location and size for distributed generations. Finally, the Bald Eagle Search algorithm was introduced in [10] for optimal placement of distributed generation with shunt reactive compensators.

On the other hand, various studies have employed different optimisation algorithms in facing multiple challenges in power sectors.

* Corresponding author.
E-mail address: zahim@umpsa.edu.my (M.Z. Sujod).

https://doi.org/10.1016/j.dajour.2023.100368
Received 2 May 2023; Received in revised form 18 August 2023; Accepted 14 November 2023
Available online 21 November 2023

Abbreviations

APL index	Active power loss index
BB-BC	Bigbang-big crunch
BFSPF	Backwards/forwardsweep power flow
DG	Distributed generation
DE	Differential evolution
DN	Distribution network
$f(s)$	Beta distribution function of solar irradiance
FA	Firefly algorithm
G	Incidentsolar irradiance (kW/m^2)
GA	Genetic algorithm
G_{ref}	Reference solar irradiance (kW/m^2)
GSA	Gravitational search algorithm
MCS	Monte Carlo simulation
MINLP	Mixed-integer non-linear programming
MILP	Mixed-integer linear programming
MVMO-SH	Hybridvariant mean–variance mapping optimisation
NOCT	Nominal operating cell temperature (°C)
$P[s]$	Probability of solar irradiance incident
PDF	Probability density function
PEM	Point estimate method
$P_i(t)$	Active powers at bus i at time segment (t)
$P_{i+1}(t)$	Active power at bus (i+1) at time segment (t)
$P_{loss,i}$	Active power loss across branch i without photovoltaic
$P_{L_k}(t, \mu_{L_k}, \sigma_{L_k})$	Active load powers at bus k (or i+1) with mean and standard deviation at segment t
$P_{Loss,pv}$	Active power loss for a system with photovoltaic
P_{PV}	Photovoltaic output power
$P_{PV}\left(t, \mu_{P_{pv,k}}, \sigma_{P_{pv,k}}\right)$	Capacity of PVDG with mean and standard deviation at segment t
PSO	Particleswarm optimisation
P_{STC}	Maximum output power at standard test conditions
p.u.	Per-unit
PV	Photovoltaic
PVDG	Photovoltaic distributed generation
$Q_i(t)$	Reactive powers at bus i at time segment t
$Q_{i+1}(t)$	Reactive power at bus (i+1) at time segment t
$Q_{L_k}(t, \mu_{L_k}, \sigma_{L_k})$	Reactive load powers at bus k (or i+1) with mean and standard deviation at segment t
RDN	Radial distribution network
RER	Renewable energy resources
R_i	Line resistance across the branch i
SFLA	Shuffled frog leaping algorithm
T_{amb}	Ambient temperature (°C)
T_{cell}	Photovoltaic cell temperature (°C)
T_{ref}	Reference temperature at standard test condition (°C)
V_{max}	Maximum voltage in per-unit
V_{min}	Maximum voltage in per-unit
X_i	Line reactance across the branch i
γ	Maximum power temperature coefficients (%/°C)
μ	Mean
σ	Standard deviation
α and β	Shape parameter of Beta PDF

For instance, [11] suggested a metaheuristics-based reactive power planning model for transmission systems. A Teaching-learning based optimisation method was employed by [12] for optimal power flow problems with stochastic wind and photovoltaics power generation. In another study, [13] used a linearised power flow model for optimal allocation and sizing of energy storage in conjunction with PV generation curtailment to meet the grid limitations and constraints.

The hybrid genetic dragonfly algorithm was utilised by [14] to solve optimal distributed generation placement and sizing. In addition, [15] proposed an Adaptive Shuffled Frogs Leaping Algorithm (ASFLA) to address network reconfiguration and distributed generation placement challenges. Another study by [16] used radial network reconfiguration to develop an improved selective binary particle swarm optimisation for power loss minimisation in 33-bus and 94-node systems. Moreover, [17] determined the best location and size of hybrid solar/hydrogen systems for rural locations using an improved harmony search and geographic information system (GIS). Lastly, [18] evaluated the impact of optimal PVDG placement and size on various aspects such as power flow, line losses, voltage profiles, and short-circuit currents. The study concluded that excessive penetration of PVDGs could lead to reverse power flow and increased power losses.

Conversely, optimal PVDG location and size can have positive impacts on power quality, voltage profiles, system reliability, and the ability to handle high loads, as indicated by studies [19,20]. To improve voltage profiles and reduce power losses in distribution networks, a multi-objective optimisation approach that combines binary particle swarm optimisation and shuffled frog leap algorithms (BPSO-SLFA) was proposed [21]. Furthermore, a multileader particle swarm optimisation (MLPSO) model was developed to optimise distributed generation in distribution networks [22]. Additionally, [23] employed the Firefly algorithm to address the allocation and sizing problem of distributed generation.

As mentioned previously, the optimal siting and sizing of PVDG in distribution system planning can be uncertain. For instance, [2] proposed an algorithm called the local particle swarm optimisation variant (LPSOV) for minimising energy loss, based on multiple load composition snapshots for the 33-bus distribution system. In another study, [24] presented a method using D-S evidence theory and affine arithmetic approaches to account for generation and load uncertainties. Meanwhile, [25] investigated distributed generation in the face of uncertainty and proposed a hybrid phasor particle swarm optimisation-Gravitational Search algorithm (PSO-GSA) method to reduce total energy loss in the distribution network. To optimise photovoltaic and wind turbine distributed generations while accounting for uncertainty, [26] presented a mixed technique using a probabilistic approach embedded in genetic algorithm (GA). Furthermore, [27] developed a GA algorithm for optimising Photovoltaic-battery system sizing for homes, taking into account the time series of solar resources and the time-of-use tariff structure to reduce energy costs. [28] construct a real options analysis model for generation growth planning under uncertain electricity demand. Finally, in a review of techniques to handle uncertainties for power systems, [29] stochastically modelled the problems associated with uncertainties, using Monte Carlo simulation, cumulant, and 2n+1-point estimation methods.

In addition to the previous studies, optimal renewable distributed generation planning in radial distribution networks was accomplished by [30] using an advanced multi-objective particle swarm optimisation method. This involved processing real-time data on wind speed and solar irradiance in a 24-hour mathematical model to compute the

Table 1
Systematic literature reviews for optimal siting and sizing of DGs in distribution system.

Article	Methodology/Algorithm	Consideration/Limitations of method			
		Considering uncertainty	Metaheuristic	Probabilistic	Analytical index
[15]	Novel Adaptive Shuffled Frogs Leaping Algorithm (ASFLA)	X	✓	X	X
[39]	Phasor PSO-GSA (PPSO-GSA)	✓	✓	✓	X
[40]	Local PSO Variant (LPSOV)	✓	✓	X	X
[41]	Analytical Hybrid PSO	X	✓	X	✓
[42]	Improved Gravitational Search Algorithm (IGSA)	X	✓	X	X
[43]	Improved Grey Wolf Optimiser, PSO, dimension learning-based hunting	X	✓	X	X
[44]	Multi-objective PSO (MOPSO)	✓	✓	X	X
[45]	Mix-Integer optimisation by GA (MIOGA)	X	✓	X	X
[46]	Mixed-integer conic programming (MICP)	✓	X	✓	✓
[47]	Honey-badger Algorithm, Combined Power Loss Sensitivity (CPLS)	X	✓	X	✓
[48]	Loss sensitivity index, Sine-cosine Algorithm	X	✓	X	✓
[8]	Severity performance index (SPI), Crow search (CS), PSO	X	✓	X	✓
[49]	Multi objective PSO	X	✓	X	X
[50]	Mixed-integer linear programming (MILP), optimal power flow (OPF)	✓	X	✓	✓
[51]	Monte-Carlo, BAB, OPF	✓	✓	✓	X
[52]	Alternative Direction Method of Multipliers (ADMM), OPF	✓	X	X	✓
[26]	Probabilistic method, GA	✓	✓	✓	X
[53]	Binary PSO, Artificial Neural Network (ANN)	✓	✓	X	X
[35]	Chance-constrained joint optimisation	✓	X	✓	X
[36]	Chance-constrained optimisation, Gaussian copula	✓	X	✓	X
[37]	Chance-constrained optimisation, GA, MINLP	✓	✓	✓	X
[54]	Teaching-Learning based optimisation	✓	✓	X	X
[55]	Stochastic-robust optimisation	✓	X	✓	X
[56]	Hybrid Moth–Flame Algorithm with Particle Swarm Optimisation	X	✓	X	X
[57]	Multi-objective thermal exchange optimisation model (MOTEO), OPF	✓	✓	✓	X
[58]	Two-stage robust optimisation, column and constraint generation, ADMM,	✓	X	✓	X
Proposed	Monte-Carlo, MVMO-SH, probabilistic BFSPF, APL Index	✓	✓	✓	✓

precise power output from these distributed generations. [31] used an Improved Whale optimisation algorithm (IWOA) to allocate hybrid photovoltaic, wind turbine, and battery storage in a 33-bus radial distribution network while also considering seasonal variations. The findings suggested that the highest losses occurred in the summer season, while the lowest losses were recorded in autumn. Solar panels, due to their low radiation, contributed less to power generation in the autumn and winter, with their most significant contribution observed in the summer and spring seasons. Additionally, [32] proposed an optimisation approach based on multi-agent clustering for wind turbines in distribution systems towards energy loss reduction. The clustering problem was solved using a genetic algorithm (GA), after which agents were assigned to each cluster, and GA was again utilised to determine the optimal sizes and placements of distributed generation in each cluster.

By contrast, power systems optimisation under uncertainty can also be achieved through robust optimisation and chance-constrained optimisation methods [33,34]. For instance, a joint optimisation algorithm that considers uncertainties was proposed by [35] to minimise power losses using network reconfigurations, capacitor banks, photovoltaics, and wind turbines in distribution networks. Meanwhile, [36] employed chance-constrained optimisation to investigate the operation of local integrated energy networks with correlated wind turbines and utilised Gaussian copula to model the uncertainty. A two-layer optimisation method was presented by [37] to determine the installation buses and sizes of electric and thermal energy storage units in the distribution network with renewable energy resources, taking into account uncertainties. The inner layer utilised chance-constrained optimisation, while the outer layer was developed using the genetic algorithm. Conversely, [38] solved the sizing capacities of renewable energy resources and transmission systems with energy storage using distributional robust optimisation.

Table 1 summarises the findings of the systematic literature as well as their limitations.

The first challenge that must be addressed in optimal photovoltaic distributed generation (PVDG) planning is the presence of uncertainties related to geographical constraints, generation, and load variation. However, there is a lack of research that explores the impact of these uncertainties on PVDG placement and sizing in the radial distribution network (RDN). Additionally, improper PVDG placement and sizing can lead to negative effects on voltage profiles and increased power losses [59], highlighting the need for an optimisation scheme that reduces power losses in the power system network. Various optimisation schemes using metaheuristics algorithms, as well as analytical and stochastic-based optimisation have been proposed by many researchers to solve distribution system planning with distributed generations. The approaches, however, were limited to dealing with constraint requirements and ignored addressing it with probabilistic variables. Furthermore, no research on the hybrid method of probabilistic–metaheuristic optimisation for PVDG planning using the Monte Carlo embedded MVMO-SH algorithm has been conducted to the authors' knowledge. The hybrid method will improve the PVDG optimisation scheme's search process. The algorithm optimises PVDG planning in an radial distribution network while considering photovoltaic generation and load uncertainty. Thus, the authors propose a hybrid method of probabilistic–metaheuristic optimisation for PVDG planning using the Monte Carlo embedded MVMO-SH algorithm, which takes into account photovoltaic generation and load uncertainty.

Another important issue is the effect of uncertainty on power flow analysis. While deterministic power flow methods assume that input variables have deterministic values, probabilistic power flow analysis is needed to consider the impact of solar resource uncertainties on load flow affected by PVDG output intermittency and load variations. The authors propose a new probabilistic backward/forward sweep power flow (BFSPF) method to evaluate fitness for optimisation and explain the influence of uncertainty in power flow with PVDG.

Previous approaches to solving distribution system planning with distributed generations have focused on constraint requirements and have ignored addressing objective functions with probabilistic variables. In contrast, the proposed probability approach can handle probabilistic variables in constraints and fitness evaluations, offering a solution to deal with uncertainty factors.

As a result, the following are the study's contributions:

1. For optimal PVDG siting and sizing in RDN considering uncertainty, a new optimisation framework based on Monte-Carlo

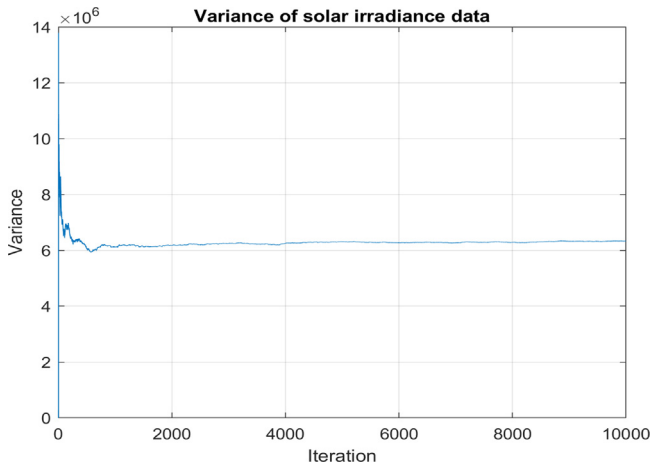

Fig. 1. Variance of solar irradiance data to determine maximum iteration in MCS.

embedded MVMO-SH is developed. The framework allows the uncertainty of photovoltaic generations and urban load demands to be emphasised based on their probability patterns.

2. PV generation uncertainty is stochastically modelled using Monte Carlo in Beta PDF for 288 segments. For residential, commercial, and industrial urban loads, the uncertainties are stochastically modelled using Monte Carlo in the Gaussian probability density function (PDF) for 288 segments. Monte Carlo allows the data to be randomly sampled and segmented into 288 segments. Each segment has its PDF patterns.
3. A new probabilistic BFSPF formulation is developed to embed the probabilistic photovoltaic generation-load model into the power flow input variables. The fitness evaluation allows optimisation problems to be solved in the face of uncertainties.
4. The active power loss (APL) index evaluates the effects of photovoltaic generation uncertainty and load variations on PVDG location and sizing.

This study investigates three (3) cases of probabilistic load models:

1. The probabilistic residential urban load model,
2. The probabilistic commercial urban load model, and
3. The probabilistic industrial urban load model.

The remaining sections are listed below. The second section goes over how to model photovoltaic generation-urban load uncertainties. Section 3 contains the optimisation strategies and problem formulations, which include mathematical models, objective functions, constraints, and the flowchart of the proposed algorithm. Finally, the findings are discussed in Section 4 using 33-bus and 69-bus radial distribution system. Finally, the discussions' outcomes and conclusions are presented.

2. Modelling of PV generation – urban load uncertainties

The solar irradiance data is obtained by clustering the weather data into twelve months. There are multiple data points at the same minute for every single day over a month. The Monte Carlo technique was used to select these weather data by randomly sampling and hourly segmenting the data sets. Each month represented a 24-hour time segment (hours) and was made up of combinational data points for the same minutes every day of the month. The data was divided into 288 segments for one year (24 h × 12 months). The variance of the data sets was used to determine the maximum iterations needed for the Monte Carlo simulation (MCS). Fig. 1 shows the variance for solar irradiance data. It has become stable after 3000 iterations.

Table 2
PV module characteristics.

PV module characteristics	Value
Maximum power, P_{max} (W)	470
Nominal operating cell temperature, NOCT (°C)	45
Maximum power current, I_{mp} (A)	10.86
Maximum power voltage, V_{mp} (V)	43.28
Short-circuit current, I_{sc} (A)	11.68
Open-circuit voltage, Voc (V)	52.14
Maximum power temperature coefficient, K_p (%/ °C)	−0.35
Current temperature coefficients, K_i (%/ °C)	0.048
Voltage temperature coefficient, K_v (%/ °C)	−0.28

The Beta PDF for each hour is expressed using Eq. (1). The probability segmentation generated by the Monte-Carlo method will affect the prediction of photovoltaic (PV) output power per panel at segment t.

$$f(s) = \begin{cases} \dfrac{\Gamma(\alpha+\beta)}{\Gamma(\alpha)\,\Gamma(\beta)} \cdot s^{(\alpha-1)} \cdot (1-s)^{(\beta-1)} & for\ 0 \le s \le 1,\ \alpha \ge 0,\ \beta \ge 0 \\ 0 & otherwise \end{cases} \tag{1}$$

To determine the shape parameters of Beta PDF, the μ, σ, α and β are derived from the following equations:

$$\mu = \frac{1}{N_d}\sum_{j=1}^{N_d} d_j \tag{2}$$

$$\sigma = \sqrt{\frac{1}{N_d}\left(d_j - \mu\right)^2} \tag{3}$$

$$\beta = (1-\mu)\cdot\left(\frac{\mu(1+\mu)}{\sigma^2} - 1\right) \tag{4}$$

$$\alpha = \frac{\mu \times \beta}{1-\mu} \tag{5}$$

The fractional probability of solar irradiance during any specific hour is derived by:

$$P[s] = \int_{s_{i,min}}^{s_{i,max}} f(s)\,ds \tag{6}$$

The PV module characteristics are tabulated in Table 2.

The cell temperature, T_{cell} derived from Eq. (7), is inserted into Eq. (8) to calculate the expected PV output per panel at time segment t, $P_{PV}(t)$.

$$T_{cell} = T_{amb} + G\left(\frac{NOCT - 20}{800}\right) \tag{7}$$

$$P_{PV} = P_{STC}\left\{\frac{G}{G_{ref}}\left[1 + \gamma\left(T_{cell} - T_{ref}\right)\right]\right\} \tag{8}$$

Based on Eqs. (7) and (8), G is the incident solar irradiance, G_{ref} is the reference solar irradiance (1 kW/m^2), $NOCT$ is the nominal operating cell temperature, T_{ref} is a reference temperature at standard test conditions in (25 °C), γ is the maximum power temperature coefficient in %/ °C, and P_{STC} is the maximum output power in Watts at standard test conditions (STC).

Realistic urban load profiles were used to account for load uncertainties. The data were obtained from Tenaga Nasional Berhad's Distribution Division, the electrical power company in Malaysia. The model was simulated using the steps listed below. First, the urban load profile data for one reference year were classified into industrial, commercial, and residential loads. The data from 15-minute intervals were divided into twelve months. For each month, there are multiple data points for similar 15-minute intervals throughout each day of the month. The Monte Carlo simulation (MCS) was performed by randomly sampling and hourly segmenting the data, representing hourly loading for each month to derive a new probabilistic load model. The data sets

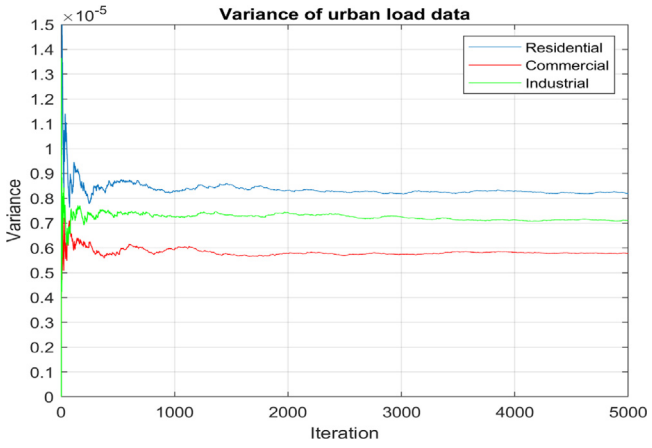

Fig. 2. Variance of urban load data to determine maximum iteration in MCS.

were divided into 288 segments (24 h × 12 months). The maximum iteration for the simulation was determined based on the variance of the data sets. Fig. 3 shows the variance became stable after 2000 iterations. Thus, the MCS for probability load models was run for 2000 iterations (see Fig. 2).

$P_L(t)$ is the load uncertainty, and it followed the normal distributions.

$$P_L(t) \sim N\left(\mu_L, \sigma_L^2\right) \tag{9}$$

The probability of each load distribution and the average urban load at the t segment is predicted as per Eqs. (10) and (11):

$$P\left[p_l\right] = \int_{p_{l_{i,min}}}^{p_{l_{i,max}}} f\left(p_l\right) dl \tag{10}$$

$$p_{l_{avg}} = \sum_{p_{l_{i,min}}}^{p_{l_{i,max}}} P\left[p_l\right] \times p_{l_i} \tag{11}$$

where $p_{l_{i,max}}$ and $p_{l_{i,min}}$ are the load demand limits that the probability of the load needing to be performed while $p_{l_{avg}}$ is the average load demand at the t-time segment.

3. Optimisation strategies

3.1. Probabilistic backward forward sweep power flow

The probabilistic power flow is designed to account for the impact of uncertainties in the input data. The equations for active and reactive powers without PV penetration can be computed using the Monte Carlo-probability density function (Monte Carlo-PDF) Monte Carlo-PDF with active and reactive input load data affected by μ and σ at the period t-segments based on the load models. A new set of probabilistic power flow equations in the RDN system can be obtained by improving the deterministic equations in backward/forward sweep power flow. The input variables, in this case, PV generation and loads, vary in 288-segments based on the probability patterns. As a result, the input variables' characters are not deterministic numbers. It can be a range of prediction values based on the probability pattern generated. Fig. 3 derives the problem formulation.

The total active and reactive power at bus i+1 without PVDG installation can be calculated as follows:

$$P_{i+1}(t) = P_i(t) - P_{L_k}(t, \mu_{L_k,t}, \sigma_{L_k,t}) - \frac{\left(P_i(t)\right)^2 + \left(Q_i(t)\right)^2}{\left|V_i(t)\right|^2} R_i \tag{12}$$

$$Q_{i+1}(t) = Q_i(t) - Q_{L_k}(t, \mu_{L_k,t}, \sigma_{L_k,t}) - \frac{\left(P_i(t)\right)^2 + \left(Q_i(t)\right)^2}{\left|V_i(t)\right|^2} X_i \tag{13}$$

where $P_{L_k}(t, \mu_{L_k,t}, \sigma_{L_k,t})$ and $Q_{L_k}(t, \mu_{L_k,t}, \sigma_{L_k,t})$ make up the active and reactive load powers at bus k (or i+1) with mean and standard deviations, μ and σ at segment t based on probabilistic load models for various customers in the load distribution. The notation t in this paper refers to the time segment which is not continuous. It has 288-time segments as explained in Section 2. Each segment has its μ_t and σ_t based on their PDF values where t denotes the time segment being used.

The equations with load variability can be utilised for PVDG integrated into the distribution system accounting for solar irradiance uncertainty. Active and reactive power outputs can be formulated using a probabilistic model of PV generation and loads in Monte Carlo-PDF based on μ and σ at segment t.

The total active and reactive powers with PVDG installation at bus i+1 can be obtained as:

$$P_{i+1}(t) = P_i(t) - P_{L_k}\left(t, \mu_{L_k,t}, \sigma_{L_k,t}\right) - P_{Loss,pv}(t) + P_{pv,i+1}\left(t, \mu_{P_{pv,i+1},t}, \sigma_{P_{pv,i+1},t}\right) \tag{14}$$

$$Q_{i+1}(t) = Q_i(t) - Q_{L_k}\left(t, \mu_{L_k,t}, \sigma_{L_k,t}\right) - Q_{Loss,pv}(t) + Q_{pv,i+1}\left(t, \mu_{Q_{pv,i+1},t}, \sigma_{Q_{pv,i+1},t}\right) \tag{15}$$

$$P_{Loss,pv}(t) = \frac{\left(P_i(t) - P_{pv,k}\left(t, \mu_{P_{pv,k},t}, \sigma_{P_{pv,k},t}\right)\right)^2 + \left(Q_i(t) - Q_{pv,k}\left(t, \mu_{P_{pv,k},t}, \sigma_{P_{pv,k},t}\right)\right)^2}{\left|V_i(t)\right|^2} R_i \tag{16}$$

$$Q_{Loss,pv}(t) = \frac{\left(P_i(t) - P_{pv,k}\left(t, \mu_{P_{pv,k},t}, \sigma_{P_{pv,k},t}\right)\right)^2 + \left(Q_i(t) - Q_{pv,k}\left(t, \mu_{P_{pv,k},t}, \sigma_{P_{pv,k},t}\right)\right)^2}{\left|V_i(t)\right|^2} X_i \tag{17}$$

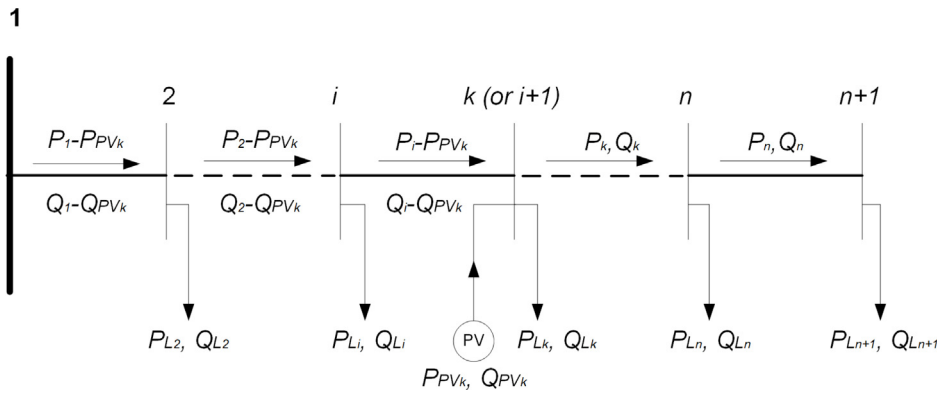

Fig. 3. The RDN system with PVDG.

$$P_{Loss,\ no\ pv}(t) = \frac{\left(P_i(t)\right)^2 + \left(Q_i(t)\right)^2}{\left|V_i(t)\right|^2} R_i \tag{18}$$

$$Q_{Loss,\ no\ pv}(t) = \frac{\left(P_i(t)\right)^2 + \left(Q_i(t)\right)^2}{\left|V_i(t)\right|^2} X_i \tag{19}$$

In this work, the assumption was made with PVDGs can inject just active power into the network. $P_{pv,k}\left(t, \mu_{P_{pv,i+1},t}, \sigma_{P_{pv,i+1},t}\right)$ and $Q_{pv,k}\left(t, \mu_{Q_{pv,i+1},t}, \sigma_{Q_{pv,i+1},t}\right)$ are obtained based on the probabilistic PV generation uncertainty model with mean and standard deviation, μ and σ at t time segment, whereas $P_{L_k}(t, \mu_{L_k,t}, \sigma_{L_k,t})$ and $Q_{L_k}(t, \mu_{L_k,t}, \sigma_{L_k,t})$ are obtained based on the probabilistic load models in 288 segments.

3.2. Objective function and constraints

The objective function is to minimise the active power loss (APL) index. The APL index can be written as in Eq. (20):

$$APL\ index = \frac{\sum_{t_{segment}=1}^{t_{segment}=288} P_{loss,pv}(t)}{\sum_{t_{segment}=1}^{t_{segment}=288} P_{loss,no\ pv}(t)} \tag{20}$$

To optimise this objective function, a probabilistic backward/forward sweep power flow (BFSPF) analysis using Monte Carlo simulation is required to obtain the expected values of active power losses at each time segment, while accounting for uncertainties in PV distributed generations and loads for each time segment t. The MVMO-SH approach is employed to locate the distributed generation at each time segment that minimise the expected power loss index over the 288-time segments. Meanwhile, equality and inequality constraints can be expressed as follows:

Network Power Balance:

The distribution power flow must satisfy the network power balance based on the non-linear equality constraints below:

$$P_i(t) + P_{pv,i+1}\left(t, \mu_{P_{pv,i+1},t}, \sigma_{P_{pv,i+1},t}\right) = P_{i+1}(t) + P_{L_k}\left(t, \mu_{L_k,t}, \sigma_{L_k,t}\right) + P_{Loss,pv}(t) \tag{21}$$

$$Q_i(t) + Q_{pv,i+1}\left(t, \mu_{Q_{pv,i+1},t}, \sigma_{Q_{pv,i+1},t}\right) = Q_{i+1}(t) + Q_{L_k}\left(t, \mu_{L_k,t}, \sigma_{L_k,t}\right) + Q_{Loss,pv}(t) \tag{22}$$

Bus Voltage Boundaries:

The safe operation boundaries must be kept for voltage at the load sites. Eq. (23) ensures the acceptable magnitude of voltages for each bus. The lower bound of voltage magnitude, V_{min} was set to be 0.95 p.u. whereas the upper bound, V_{max} is set to be 1.05 p.u.

$$V_{min} \le |V_i| \le V_{max} \qquad i = 1, 2, \ldots, n\ bus \tag{23}$$

PVDG Operating Capacity:

The PVDG capacity limit is determined by the inequality constraint listed below. $P_{PV\,DG}^{min}$ capacity is equal to zero, whereas $P_{PV\,DG}^{max}$ capacity is determined by the probability t-segment of the total active load demand. Thus, the capacity of $P_{PV\,DG}^{max}$ for different customers will vary depending on the total active power load for those customers.

$$P_{PV\,DG}^{min}\left(t, \mu_{P_{pv,i+1},t} - \sigma_{P_{pv,i+1},t}\right) \le P_{PV\,DG}\left(t, \mu_{P_{pv,i+1},t}, \sigma_{P_{pv,i+1},t}\right) \le P_{PV\,DG}^{max}\left(t, \mu_{P_{pv,i+1},t} + \sigma_{P_{pv,i+1},t}\right) \tag{24}$$

The penetration limit of PVDG in the distribution system must satisfy the following equation:

$$\sum_{i=1}^{n} P_{PV\,DG,i}\left(t, \mu_{P_{pv,i+1},t}, \sigma_{P_{pv,i+1},t}\right) \le \sum_{i=1}^{n} P_{Load,i}\left(t, \mu_{P_{pv,i+1},t}, \sigma_{P_{pv,i+1},t}\right), \tag{25}$$

with $i = 1, 2, \ldots, n\ bus$

PVDG Location:

The PVDG location can be linked to any bus in the system except at the slack bus:

$$2 \le PV\,DG_{location} \le \max\ no.of\ buses \tag{26}$$

Branch Current Limits:

The branch's current limit is given by:

$$0 \le I_{ik}(t) = \sqrt{\frac{\left(P_{i-1}^2(t) + Q_{i-1}^2(t)\right)}{V_{i-1}^2(t)}} \le I_{ik}^{max}(t) \tag{27}$$

3.3. Monte Carlo embedded MVMO-SH

The MVMO-SH algorithm is a hybrid of the swarm and stochastic optimisation methods. Based on the mean and variance of the n-best population, the MVMO-SH algorithm was developed. The genes of the offspring generation are mutated using the n-best population's strategic transformation of mean–variance mapping. MVMO-SH is an MVMO swarm operation composed of a group of NP particles carrying its memory for global searching via an improved scheme of classic MVMO. The variable searching space for optimisation is normalised to [0, 1] interval ranges, but the function evaluation uses its problem ranges. The MVMO-SH algorithm's basic principles can be found in [60–64]. The optimisation problem is solved using a new development of Monte-Carlo embedded MVMO-SH, and the fitness evaluation is generated using the probabilistic BFSPF algorithm. The number of particles for the swarm operation was set to 50. The FS factor was set to 1, the increment, Δd was 0.05 and initial value, d_i was 1. Given i as fitness evaluation, k as particle counters, m as the maximum number of iteration and N_p as the number of particles. The maximum evaluation was set to 100 iterations. The detailed procedure is as follows:

Step 1: Parameter initialisations.

Step 2: Data loading for solar irradiance and urban load distribution.

Step 3: The Monte Carlo probabilistic urban load models (288, 2000) for residential, commercial, and industrial loads are generated.

Step 4: The probabilistic PV uncertainty model is generated using Monte Carlo-Beta PDF (288, 3000). Steps 3 and 4 are depicted in Fig. 4.

Step 5: Radial case system is loaded, and the feasibility of acquiring active power losses using probabilistic BFSPF for the case without PVDG penetrations is tested using Monte Carlo. The bus data is being replaced with new load data which is the multiplication of old load data and the probabilistic load model based on Monte Carlo-PDF which is influenced by the μ and σ in 288 segments.

Step 6: MVMO-SH generates numbers at random based on the variables [0,1].

Step 7: To perform the fitness evaluations, the variables are de-normalised from [0,1] to their original boundary.

Step 8: The PVDG location and size are specified by MVMO-SH, and the probability is checked using Monte Carlo.

Step 9: The fitness values in the individual archive will be updated, filled, and saved. The process for determining PVDG location and size using Np particle classification and parent selection is being updated. The parent archive is the best solution archive. The archive's mean and variance are computed. Mapping means and variance value dimensions allow for cross-over and mutation. The candidate solutions/fitness values will be updated/filled/stored in the personal archive. The archive's mean and variance will be calculated. The solution archive will be updated to include the best solutions so far in the first row. If the solution

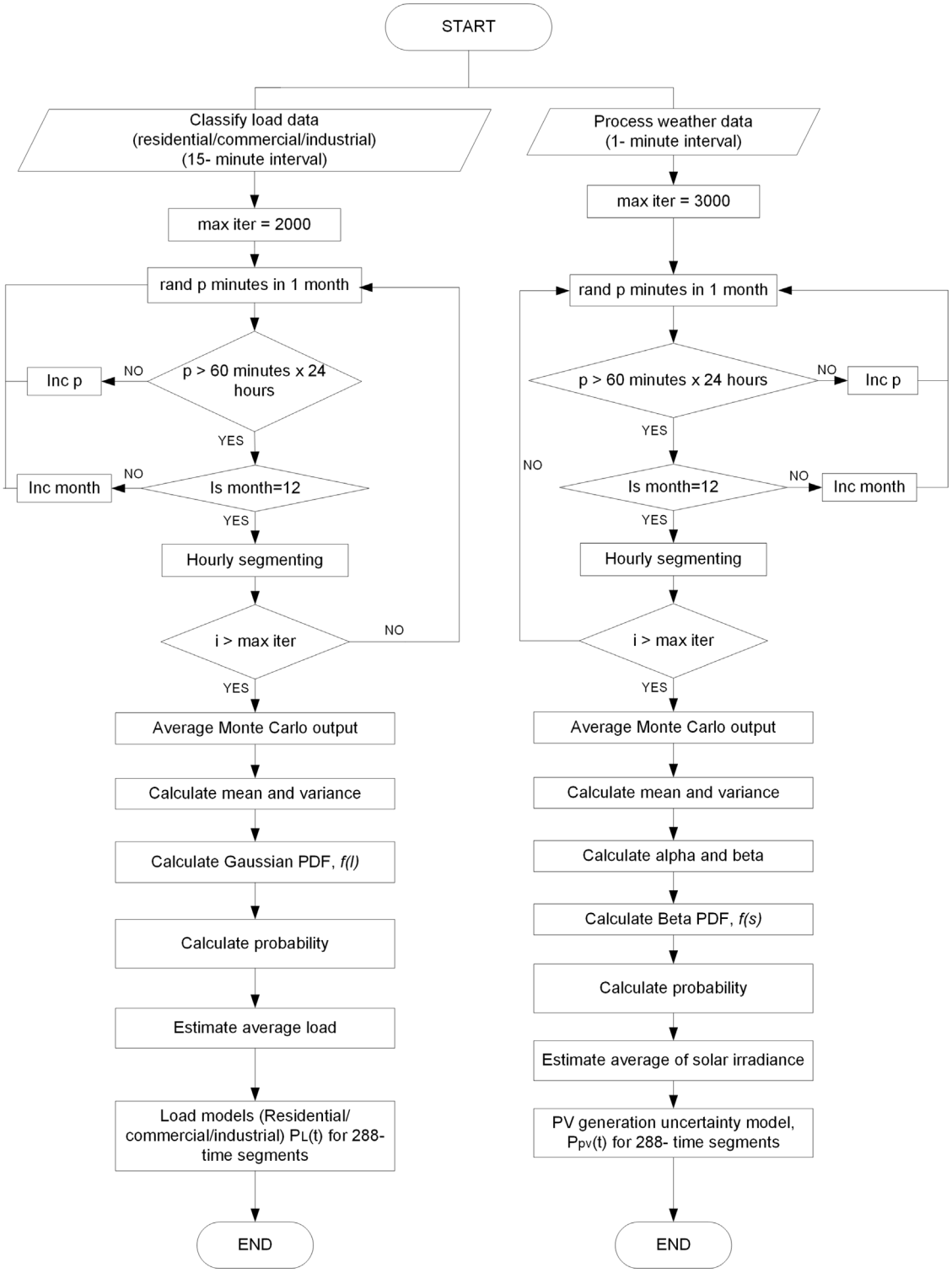

Fig. 4. Probabilistic PV generation-load model based on Monte Carlo – PDF method.

archive's table is full, the infeasible value is replaced with the possible value. If there are two possible values, the best one is chosen. If two infeasible values exist, the one with the lower violation is chosen. The reproduction is then determined. The parent archive is the best solution archive. Mapping the dimensions based on the mean and variance allows for cross-over and mutation.

Step 10: Steps 6 through 9 must be repeated for m iterations. The optimisation process is terminated if the termination criteria are met. Otherwise, the procedures are repeated.

Step 11: Printed total power losses, an index of active power loss, and voltage profiles with PVDG penetrations.

Step 12: The APL index with the lowest value indicates the best location and size for PVDG integration in RDN. Fig. 5 depicts a flowchart for PVDG planning in an RDN system while accounting for PV generation and urban load uncertainties.

3.4. Monte Carlo embedded GA (Monte Carlo-GA)

In the initialisation step, the GA was carried out to do the optimisation with a population size of 50 individuals. These individuals will be classified and ranked based on the value of their fitness. The number of variables was set to 2, the migration fraction was 0.2, and crossover fraction was 0.8. Steps 1 through step 5 in Section 3.3 are the same for Monte Carlo-GA's procedures. After step 5, the proceeding is as follows:

Step 6: GA generates random chromosomes for each of the 50 individuals in the population.

Step 7: The chromosomes were validated and updated by checking their constraints and computing the fitness function.

Step 8: The PVDG location and size are specified by GA, and the probability is checked using Monte Carlo.

Step 9: The process for determining PVDG location and size using parent selection is being updated. allow for cross-over and mutation. GA will go through the steps of selecting, and reproducing each chromosome, repeatedly updating them until the best solution is found. The candidate solutions/fitness values will be updated. High-fitness individuals are more likely to be chosen for reproduction allows for cross-over and mutation. The process for determining PVDG location and size is being updated.

Step 10: Steps 6 through 9 must be repeated until the population has converged. The optimisation process is terminated if the termination criteria are met.

Step 11: Printed total power losses, an index of active power loss, and voltage values for all buses.

Step 12: The APL index with the lowest value indicates the best location and size for PVDG integration in RDN.

3.5. Monte Carlo embedded PSO (Monte Carlo-PSO)

In the initialisation step, the PSO was carried out to do the optimisation with a population size or swarm of 50. The inertia weight, ω is randomly selected between 1.0 and 0.3. The PSO's basic principles can be found in [65]. For the Monte Carlo – PSO procedures, steps 1 until 5 in Section 3.3 are similar. After step 5, the proceeding is as follows:

Step 6: The particle population is initialised with randomly generated positions and velocities to explore the solution space.

Step 7: The fitness of each particle was validated. The personal best (pbest) and global best (gbest) were determined to evaluate the fitness function.

Step 8: The PVDG location and size are specified by PSO, and the probability is checked using Monte Carlo.

Step 9: The process for determining PVDG location and size is updated by updating the velocity and position: The velocity and position of each particle are updated based on the current fitness and the best fitness that has been found so far. The velocity update involves combining the current velocity with the attraction to the best position found by the particle and the best position found by the entire swarm. The position update involves applying the updated velocity to the current position of the particle.

Step 10: Steps 6 through 9 must be repeated until the value converged. The optimisation process is terminated if the termination criteria are met.

Step 11: Printed total power losses, an index of active power loss, and voltage values for all buses.

Step 12: The APL index with the lowest value indicates the best location and size for PVDG integration in RDN.

4. Results and discussion

4.1. Probabilistic PV generation – urban load uncertainty model

Figs. 6 through 9 depict the probabilistic uncertainty model in 288 segments via Monte Carlo simulation (MCS) generated based on μ and σ of each time segment.

From the Monte Carlo derivation, the μ, σ, α, and β of the hourly solar irradiance were calculated to derive the shape parameter of the Beta probability density function (Beta PDF). Fig. 10 shows the sample of Beta PDF in segments 81, 84, 86 and 90. Since the data was split into 288 segments (24 h × 12 months), the sample of Beta PDF for solar irradiance in segments 81, 84, 85, 88, and 90 represented April at 9 a.m., 12 p.m., 1 p.m., 4 p.m., and 6 p.m.

The outcome demonstrated that intense solar radiation with a high probability density of solar irradiance occurred during noon (segments 84 and 85). The Beta PDF plot for segments 84 and 85 (noon) showed higher probability density with intense solar irradiance compared to the results for segment 81 (morning) and segments 88 and 90 (evening). The results demonstrate the versatility of the Beta curve for modelling solar irradiance uncertainty which allows it to represent the probability density of the data shapes for all 288 segments.

Beta PDF was used to derive the probability of solar irradiance and calculate the probabilistic uncertainty model of photovoltaic generation for 288-segments. The PV generation output was based on the uncertainty model of solar irradiance in 288 segments generated scenarios. Since the historical weather data were based on the case study in Tropical Climate conditions, the variations of ambient temperatures were not significant. Hence, the uncertainty of ambient temperature was determined based on the averaging method. The expected photovoltaic output per panel at each time segment was obtained based on Eq. (8). The PV module characteristics were tabulated in Table 2. Accordingly, the Beta PDF for PV output per panel can also be obtained. Fig. 11 depicts the sample of Beta PDF for photovoltaic output power per panel in segments 81, 84, 85, 88, and 90 represented April at 9 a.m., 12 p.m., 1 p.m., 4 p.m., and 6 p.m. The Beta PDF plot for segments 84 and 85 (noon) showed higher PV-generated powers compared to the results for segments 81 (morning) and segments 88 and 90 (evening). The curves vary according to the probability segmentation of solar irradiance generated by Monte Carlo – Beta PDF.

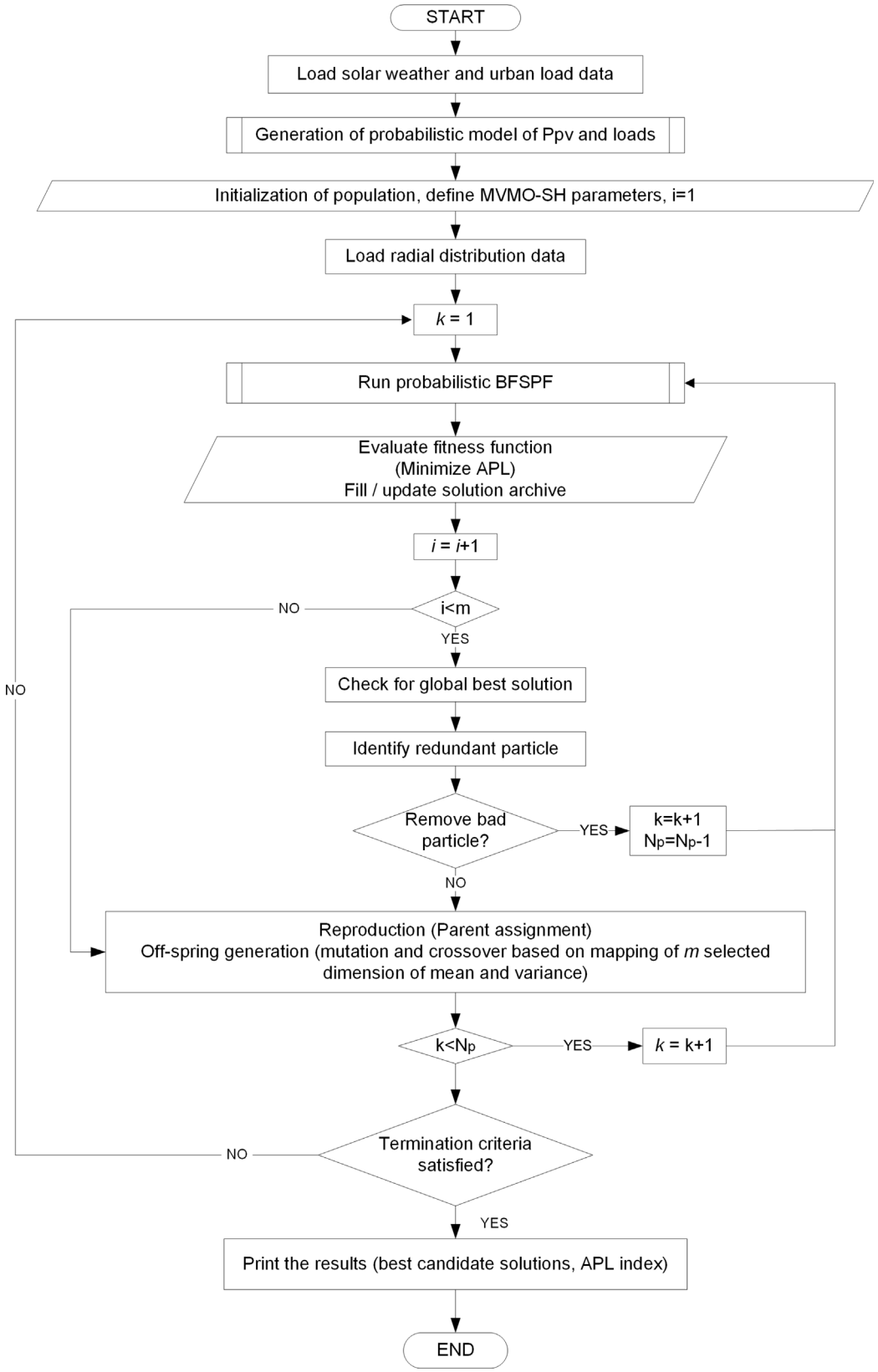

Fig. 5. Optimisation of PVDGs in RDN With i is the iteration counters, k is the particle counters, Np is the number of particles and m is the number of the iterations.

The residential, commercial, and industrial urban load uncertainties were modelled in almost the same procedures as the PV generation model. Fig. 12 depicts the PDF curve of the urban load uncertainty for residential, commercial, and industrial at segment 86. The residential, commercial, and industrial loads' coefficients of variation (CV) were 2.63%, 2.1308% and 2.5632%, respectively. It is reasonable to

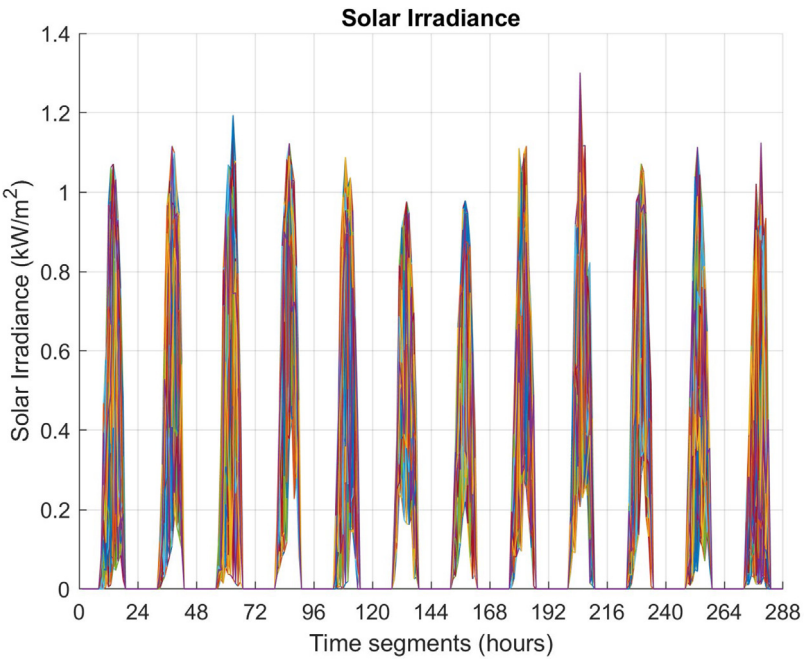

Fig. 6. Probabilistic solar irradiance uncertainty model in 288 segments using MCS.

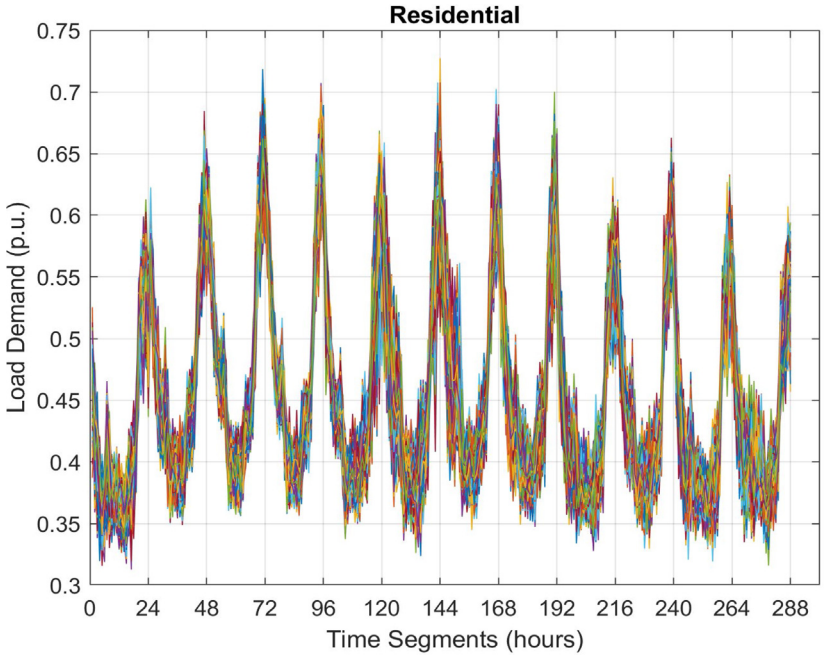

Fig. 7. Probabilistic residential urban load uncertainty model in 288 segments using MCS.

conclude that the illustrated PDF curves are characterised by Gaussian probability density.

The results of the probabilistic PV generation-urban load uncertainty model, which is affected by μ and σ at segment t for the 288 segments, will be embedded into Eqs. (12) to (27) for fitness evaluations of the optimisation problems.

4.2. Optimal siting and sizing of PVDG

The simulations were carried out for a single PVDG unit and multiple PVDG units in the standard 33 bus and 69 bus RDN. Figs. 13 and 14 illustrate the topology. The 33 bus RDN has 3715 kW and 2300 kVar loads. The 69 bus RDN has loads of 3800 kW and 2690 kVar.

Table 3 shows the impact of uncertainties in PVDG locations and sizes in the 33-bus RDN. The results for all load models namely residential, commercial and industrial showed that the optimal PVDG location was bus no. 6 for 1 PVDG unit. For two PVDG units, the optimal locations were bus nos. 6, and 14 in the residential load model, and bus nos. 6, and 16 for commercial and industrial load models, respectively. For 3 PVDG units, the optimal locations were bus nos. 6, 14, and 25 in the residential load model, and bus nos. 6, 16, and 25 for the commercial and industrial load models. From the observations of optimal PVDG sizes in 33-bus RDN, the PVDGs sites and sizes are different depending on the load patterns. The MVMO-SH method has been employed successfully to optimise the PVDG size and location in

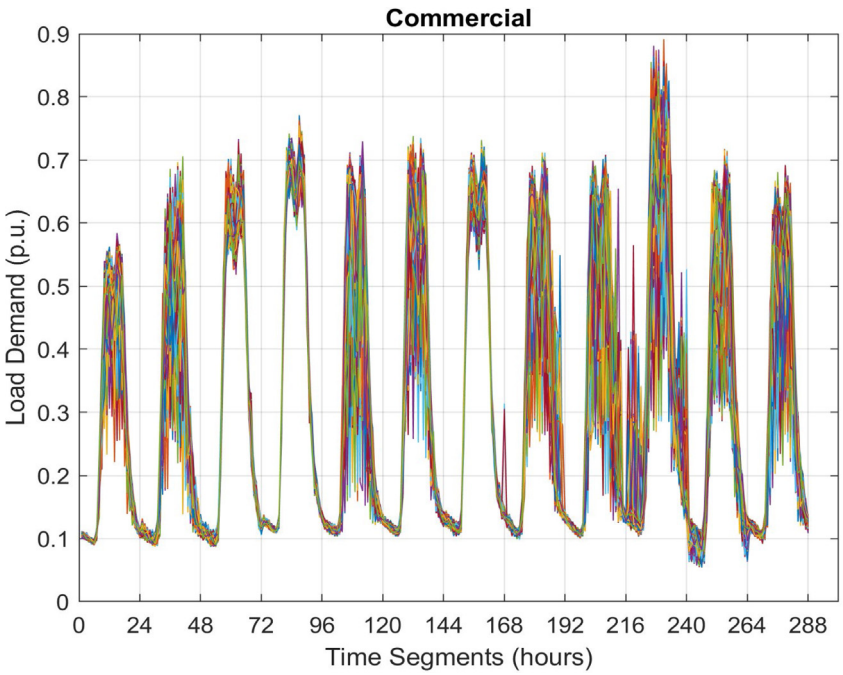

Fig. 8. Probabilistic commercial urban load uncertainty model in 288 segments using MCS.

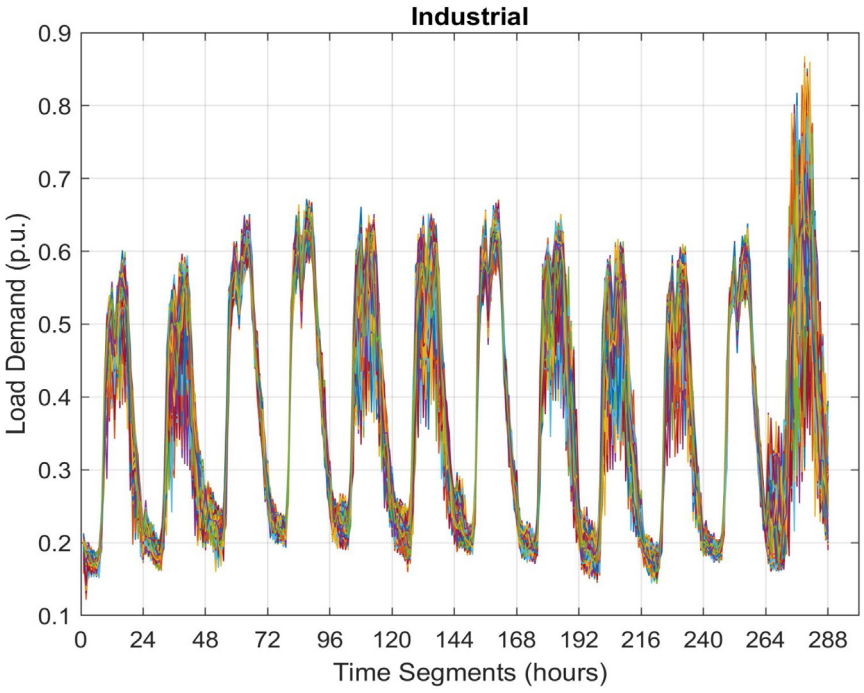

Fig. 9. Probabilistic industrial urban load uncertainty model in 288 segments using MCS.

the radial network with the smallest APL index compared to PSO and GA.

Table 4 shows the comparison of APL index reduction in 33-bus RDN considering uncertainties. Based on the results obtained, there was a significant reduction in the APL index for the case of 3 PVDGs compared to the system without PVDG for all load models examined.

The impact of uncertainties in PVDG optimal locations and sizes in the 69-bus test system is shown in Table 5. The optimisations for 1 to 3 PVDG units produce comparable results for PVDG sites and sizes when using MVMO-SH, PSO, and GA. For the case of a single PVDG unit, the proposed PVDG location for all load models was bus no. 61. For the case of two PVDGs, the optimal PVDG locations for commercial load models were bus nos. 61 and 18, while the locations for residential and industrial load models were bus nos. 61 and 17. For all optimisation approaches, the optimal PVDG locations in residential urban load RDN were bus nos. 61, 17, and 9. However, in terms of commercial urban load, bus routes 61, 18, and 11 were the best. Furthermore, for all optimisation approaches used, the optimal locations for the case of

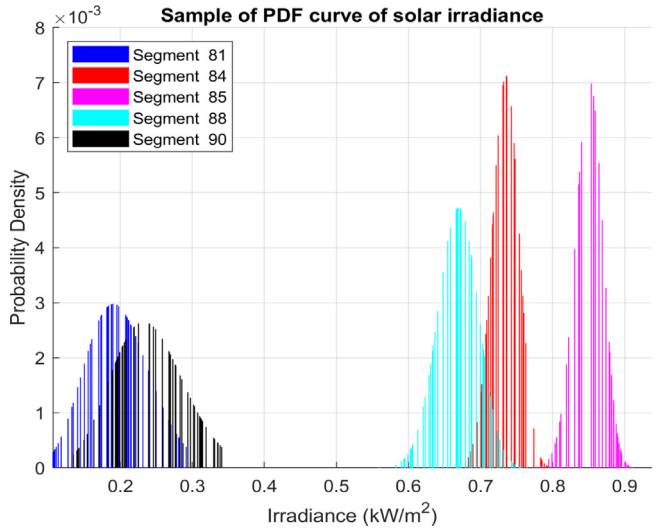

Fig. 10. PDF curve of solar irradiance at Segments 81, 84, 85, 88, and 90.

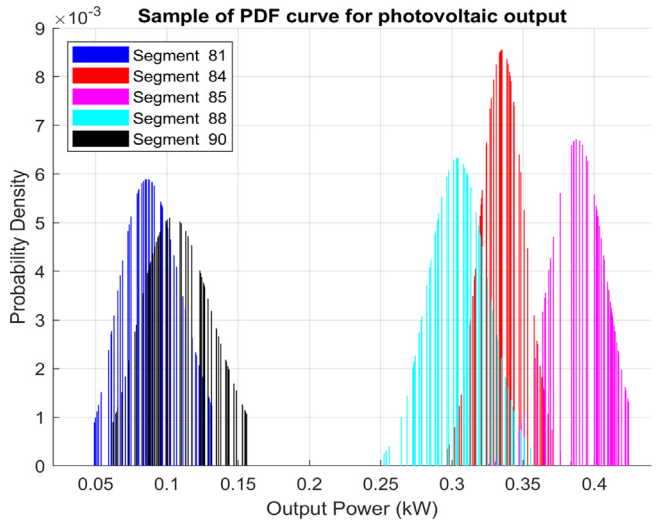

Fig. 11. PDF curve for PV output powers at segments 81, 84, 85, 88, and 90.

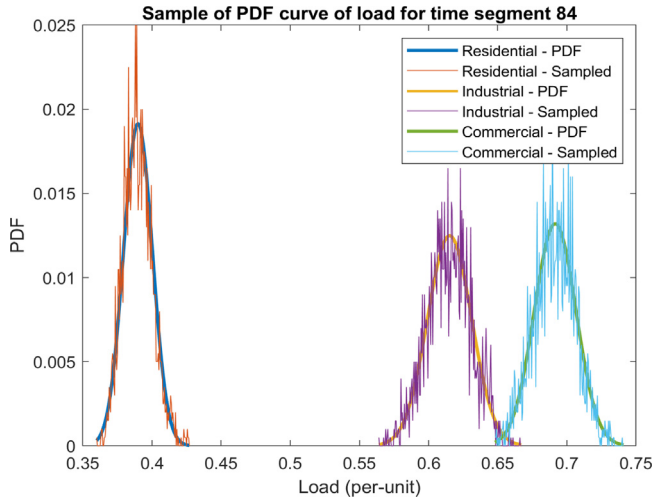

Fig. 12. PDF curve for residential, commercial, and industrial urban load at segment 84.

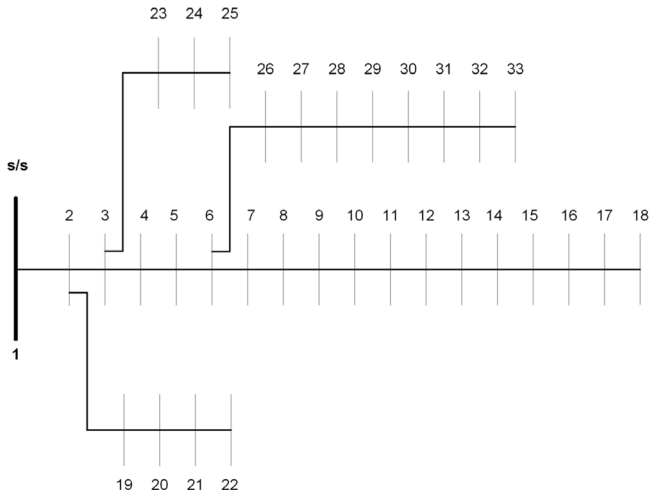

Fig. 13. The 33-bus RDN schematic.

Table 3
Comparison of optimal location and sizing considering uncertainties in PVDG generation — Urban load models for 33-bus R.

Case	Residential Urban Load Model		
	MVMO-SH	PSO	GA
PVDG Size (MW) and Location (Bus)	1.9623 (6) 0.4910 (14) 0.5785 (25)	1.9685 (6) 0.4829 (14) 0.5822 (25)	1.9684 (6) 0.4829 (14) 0.5822 (25)
Total PVDG Size (MW)	3.0318	3.0336	3.0335
APL Index	0.4094	0.4095	0.4095
Case	Commercial Urban Load Model		
	MVMO-SH	PSO	GA
PVDG Size (MW) and Location (Bus)	2.9032 (6) 0.4289 (16) 0.3773 (25)	2.9046 (6) 0.4295 (16) 0.3809 (25)	2.9043 (6) 0.4294 (16) 0.3812 (25)
Total PVDG Size (MW)	3.7094	3.7150	3.7149
APL Index	0.4811	0.4812	0.4811
Case	Industrial Urban Load Model		
	MVMO-SH	PSO	GA
PVDG Size (MW) and Location (Bus)	2.7812 (6) 0.4324 (16) 0.5011 (25)	2.7809 (6) 0.4388 (16) 0.4953 (25)	2.7812 (6) 0.4386 (16) 0.4952 (25)
Total PVDG Size (MW)	3.7147	3.7150	3.7150
APL Index	0.4655	0.4659	0.4659

industrial urban load RDN were bus nos. 61, 17, and 11. According to Table 5, the MVMO-SH method produces the smallest PVDG size when compared to PSO and GA.

The findings also show that uncertainties affect the optimal location and size of multiple PVDGs. The observations of optimal PVDG sizes in 69-bus RDN for various load models show that PVDG penetration levels vary according to load patterns. PVDG penetration levels are highest in commercial loads, followed by industrial loads, and lowest in residential loads.

Table 6 summarises the APL index comparison in the 69-bus RDN considering the uncertainties. The results showed that the MVMO-SH method produced the lowest APL index compared to PSO and GA. The results also showed that the APL index in the RDN system with multiple PVDGs was significantly lower than in the system without PVDGs. For multiple PVDG planning, the APL index steadily decreased. The reduction in the APL index for multiple PVDG planning is most likely caused by increasing the injected active power by PVDGs connected directly to distribution network loads, resulting in less current flowing

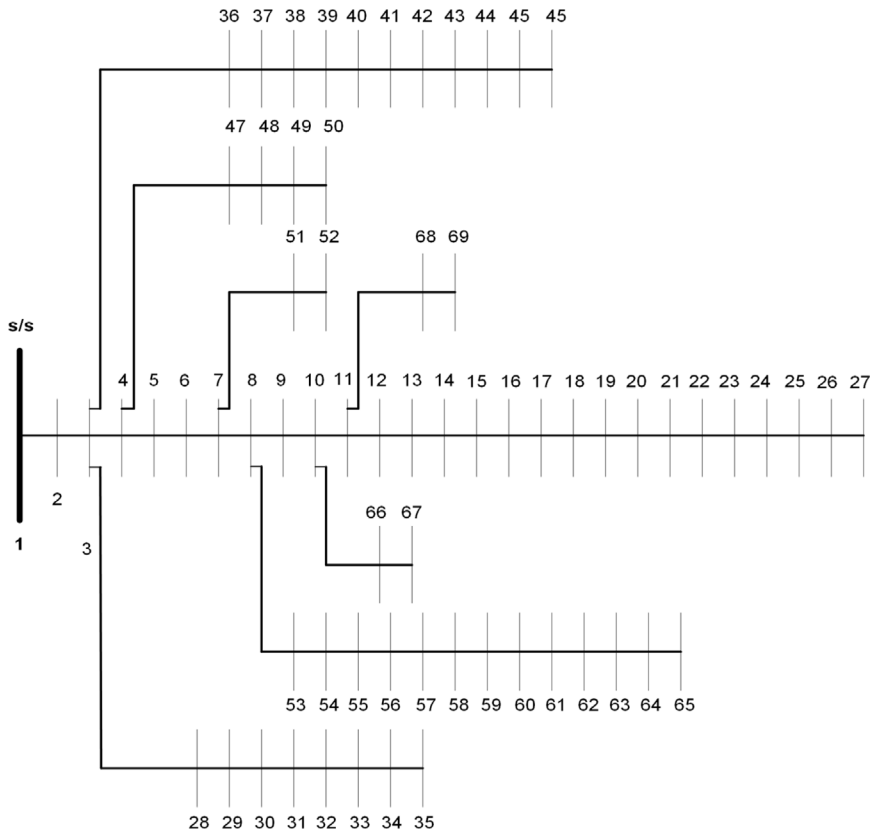

Fig. 14. The 69-bus RDN schematic.

Table 4
Comparison of APL index considering uncertainties in PVDG generation — Urban load models for 33-bus RDN.

Case study	Methods					
	MVMO-SH		PSO		GA	
Residential	APL Index	% APL Reduction	APL Index	% APL Reduction	APL Index	% APL Reduction
0 PVDG	1.0	–	1.0	–	1.0	–
1 PVDG	0.5652	43.48	0.5662	43.38	0.5661	43.39
2 PVDG	0.4582	54.18	0.4583	54.17	0.4583	54.17
3 PVDG	0.4094	59.06	0.4095	59.05	0.4095	59.05
Commercial	APL Index	% APL Reduction	APL Index	% APL Reduction	APL Index	% APL Reduction
0 PVDG	1.0	–	1.0	–	1.0	–
1 PVDG	0.5540	44.60	0.5541	44.59	0.5541	44.59
2 PVDG	0.5058	49.42	0.5076	49.24	0.5076	49.24
3 PVDG	0.4811	51.89	0.4812	51.88	0.4811	51.89
Industrial	APL Index	% APL Reduction	APL Index	% APL Reduction	APL Index	% APL Reduction
0 PVDG	1.0	–	1.0	–	1.0	–
1 PVDG	0.5501	44.99	0.5503	44.97	0.5503	44.97
2 PVDG	0.4954	50.46	0.4971	50.29	0.4971	50.29
3 PVDG	0.4655	53.45	0.4659	53.41	0.4659	53.41

through the branches and thus less total power loss in the network. The optimal PVDGs planning in this work was limited to three PVDGs.

Tables 7 and 8 show the minimum voltage values in the presence of uncertainties in 33-bus and 69-bus RDN, respectively. In the 33-bus without PVDG, the critical voltage is located at bus no. 18, whereas in the 69-bus without PVDG, the critical voltage is located at bus 65. The voltage values in the case of 33-bus RDN are 0.9298 p.u. (residential urban load), 0.9244 (commercial), and 0.9314 p.u. (industrial), respectively; which fall below the desired minimum voltage level, which is set to 0.95 p.u. Whereas, in the case of 69-bus RDN, the voltage values are 0.9330 p.u. (residential urban load), 0.9282 (commercial), and 0.9347 p.u. (industrial), respectively. The magnitude of the voltage improved significantly within the permissible limits for the system connected to multiple PVDGs. To avoid over-voltage due to oversized PV, the bus voltage boundaries for safe operation limits must be kept for voltages at the load sites for the system with PVDGs. The lower bound and upper bound of voltage, in Eq. (23) ensures the acceptable magnitude of voltages for each bus in the system with PVDGs.

Fig. 15 depicts the assessment of voltage fluctuations in 69-bus RDN for the system without PVDG. The uncertainty could result in voltage deviation and rapid voltage fluctuations, leading to voltage violations and reduced power quality if it is not properly managed. To ensure

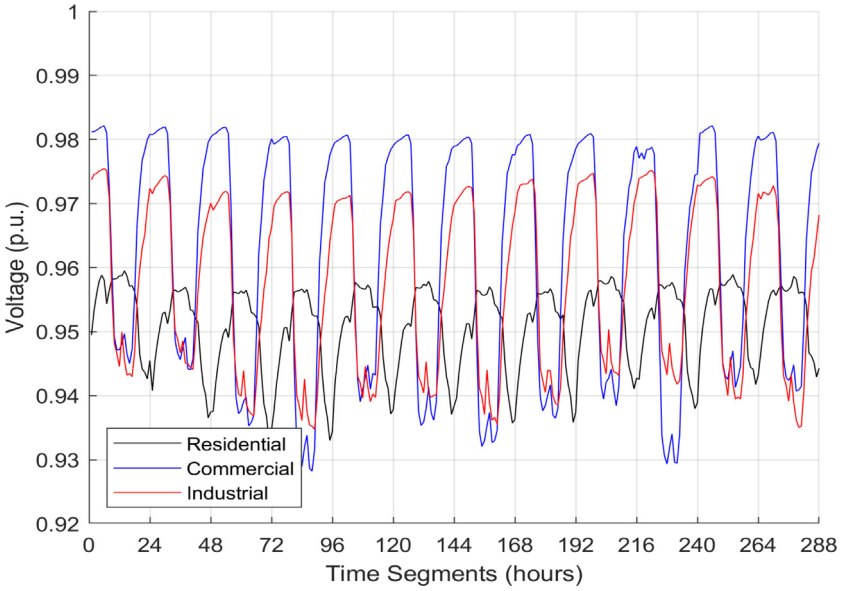

Fig. 15. Impact of uncertainty on voltage Variations in 69-bus RDN.

Table 5
Comparison of optimal location and sizing considering uncertainties in PVDG generation — Urban load models for 69-bus RDN.

Case	Residential Urban Load Model		
	MVMO-SH	PSO	GA
PVDG Size (MW) and Location (Bus)	1.4908 (61) 0.4552 (17) 0.5892 (9)	1.4571 (61) 0.4461 (17) 0.6347 (9)	1.4568 (61) 0.4462 (17) 0.6340 (9)
Total PVDG Size (MW)	2.5352	2.5379	2.5370
APL Index	0.3403	0.3409	0.3409
Case	Commercial Urban Load Model		
	MVMO-SH	PSO	GA
PVDG Size (MW) and Location (Bus)	2.0995 (61) 0.5426 (18) 0.2073 (11)	2.1383 (61) 0.5423 (18) 0.1658 (11)	2.1382 (61) 0.5423 (18) 0.1695 (11)
Total PVDG Size (MW)	2.8494	2.8464	2.8500
APL Index	0.3570	0.3619	0.3618
Case	Industrial Urban Load Model		
	MVMO-SH	PSO	GA
PVDG Size (MW) and Location (Bus)	2.0255 (61) 0.5319 (17) 0.2302 (11)	2.0500 (61) 0.5321 (17) 0.2133 (11)	2.0504 (61) 0.5333 (17) 0.2115 (11)
Total PVDG Size (MW)	2.7876	2.7954	2.7952
APL Index	0.3504	0.3530	0.3531

reliable, efficient, and safe operations of the power system, the impacts of uncertainty need to be measured in the power system planning.

Figs. 16 to 18 show the convergence results for residential, commercial, and industrial urban load models in 69-bus RDN. In terms of convergence performance, the MVMO-SH algorithm outperforms PSO and GA in solving the optimisation problem with a minimum APL index at high convergence rates. Because of the algorithm's generic features, which can be easily embedded, MVMO-SH is more robust than PSO and GA to integrate the routines into the probabilistic power flow scheme. The performance speed of MVMO-SH, PSO and GA for DG optimisation in 69-bus RDN without considering uncertainty was presented in our work in [66]. MVMO-SH offers quick execution with total simulation times of 0.55 s while PSO and GA are 13.87 s and 80.72 s, respectively. To evaluate the performance speed of MVMO-SH, PSO, and GA for PVDG optimisation in 69-bus RDN in the presence of uncertainty, the total simulation times are increased due to the computational burden to generate probabilistic uncertainty models and evaluate fitness functions in 288 segments. In one trials of optimisation process, the simulation times of MVMO-SH, PSO, and GA for 3 PVDGs installation in 69-bus RDN for residential urban load model were 1155.67 s, 7501.05 s, and 9887.16 s, respectively; run on HP Victus laptop, AMD Ryzen 5 5600H with Radeon Graphics 3.30 GHz, 16 GB RAM. The results show that the MVMO-SH method provides the fastest convergence rate while minimising the APL index.

In addition, metaheuristics optimisation provides accurate and reliable solutions for optimal PVDG size and placement in the distribution network. Since this work involved making optimal decisions in the presence of uncertainty, Monte Carlo embedded MVMO-SH offers hybridisation with the probabilistic method to deal with stochastic variables in constraints and fitness evaluations. Thus, the impacts of uncertainty can be measured. Monte Carlo simulation allows uncertain parameters, which are load variability, photovoltaic generation outputs, and distribution line parameters by creating multiple segmentations via probability density functions. This allows for the optimisation process to be conducted by MVMO-SH for different time segments, capturing the variations over time. The Monte Carlo embedded MVMO-SH algorithm can make accurate decisions and ensure that the solution remains valid in a variety of potential operational conditions by taking uncertainties and possible risks into the system, making it applicable to a wide range of power system planning and operations.

Table 9 presents statistical assessments for three PVDGs in a 69-bus RDN as additional evidence of MVMO- SH's ability to deliver the best solutions to the objective function. With the risk of uncertainties in mind, the statistical analysis of the standard deviations (SD), best value (BV), and worst value (WV) of the objective functions were evaluated in 20 trials for the optimisation process to validate the results and increase accuracy in the optimal solutions. The BV and WV showed convergence ability, whereas the SD showed method stability [67]. In comparison to the GA and PSO methods, the MVMO-SH has the lowest BV and WV, as shown in Table 5. In the residential case, the BVs were 0.3403 (MVMO-SH) and 0.3409 (GA/PSO), while in the commercial case, the BVs were 0.3570 (MVMO-SH) and 0.3618 (GA/PSO). In the industrial sector, the BVs were 0.3504 (MVM)-SH, 0.3531 (GA), and 0.3530 (PSO). Furthermore, the WVs in the residential case were 0.3587 (MVMO-SH) and 0.3588 (GA/PSO), whereas the WVs in the commercial case

Table 6
Comparison of APL index considering uncertainties in PVDG generation — Urban load models for 69-bus RDN.

Case study	Methods					
	MVMO-SH		PSO		GA	
Residential	APL Index	APL Reduction (%)	APL Index	APL Reduction (%)	APL Index	APL Reduction (%)
0 PVDG	1.0	–	1.0	–	1.0	–
1 PVDG	0.4194	58.06	0.4197	58.03	0.4197	58.03
2 PVDG	0.3585	64.15	0.3587	64.13	0.3588	64.12
3 PVDG	0.3403	65.97	0.3409	65.91	0.3409	65.91
Commercial	APL Index	APL Reduction (%)	APL Index	APL Reduction (%)	APL Index	APL Reduction (%)
0 PVDG	1.0	–	1.0	–	1.0	–
1 PVDG	0.4057	59.43	0.4056	59.44	0.4056	59.44
2 PVDG	0.3625	63.75	0.3629	63.71	0.3629	63.71
3 PVDG	0.3570	64.30	0.3618	63.82	0.3618	63.82
Industrial	APL Index	APL Reduction (%)	APL Index	APL Reduction (%)	APL Index	APL Reduction (%)
0 PVDG	1.0	–	1.0	–	1.0	–
1 PVDG	0.3989	60.62	0.4007	59.93	0.4007	59.93
2 PVDG	0.3546	64.54	0.3551	64.49	0.3552	64.48
3 PVDG	0.3504	64.96	0.3530	64.70	0.3531	64.69

Table 7
Comparison of Minimum Voltage Values Considering Uncertainties in 33-bus RDN.

Case	Residential Urban Load Model			
	Without PVDG	1 PVDG	2 PVDGs	3 PVDGs
Minimum voltage value (p.u) and location (Bus)	0.9298 (18)	0.9580 (18)	0.9698 (33)	0.9716 (33)
Case	Commercial Urban Load Model			
	Without PVDG	1 PVDG	2 PVDGs	3 PVDGs
Minimum voltage value (p.u) and location (Bus)	0.9244 (18)	0.9636 (18)	0.9761 (33)	0.9772 (33)
Case	Industrial Urban Load Model			
	Without PVDG	1 PVDG	2 PVDGs	3 PVDGs
Minimum voltage value (p.u) and location (Bus)	0.9314 (18)	0.9662 (18)	0.9774 (33)	0.9787 (33)

Table 8
Comparison of minimum voltage values considering uncertainties PVDG generation — Urban load models in 69-bus RDN.

Case	Residential Urban Load Model			
	Without PVDG	1 PVDG	2 PVDGs	3 PVDGs
Minimum voltage value (p.u) and location (Bus)	0.9330 (65)	0.9773 (65)	0.9791 (65)	0.9821 (65)
Case	Commercial Urban Load Model			
	Without PVDG	1 PVDG	2 PVDGs	3 PVDGs
Minimum voltage value (p.u) and location (Bus)	0.9282 (65)	0.9792 (65)	0.9934 (65)	0.9940 (65)
Case	Industrial Urban Load Model			
	Without PVDG	1 PVDG	2 PVDGs	3 PVDGs
Minimum voltage value (p.u) and location (Bus)	0.9347 (65)	0.9808 (65)	0.9926 (65)	0.9931 (65)

were 0.3625 (MVMO-SH) and 0.3629 (GA/PSO). The WVs in the industrial load were 0.3521 (MVM)-SH and 0.3552 (GA/PSO). Again, the statistical results showed that the MVMO-SH algorithm is superior.

5. Conclusion

A new optimisation framework, utilising the Monte Carlo embedded MVMO-SH algorithm, was developed to address uncertainties and optimise PVDG placement and sizing in the RDN system network, with a focus on minimising the APL index. The effectiveness of the proposed framework was validated through testing on 33-bus and 69-bus RDN systems. A new formulation of probabilistic BFSPF in 288-segmentation was developed based on PV generation-load uncertainties at t-segments. The proposed optimisation framework was tested in three urban load cases, i.e., residential, commercial, and industrial, to assess the effectiveness of the proposed method with both single and multiple PVDG units. The study revealed that uncertainties affect the optimal

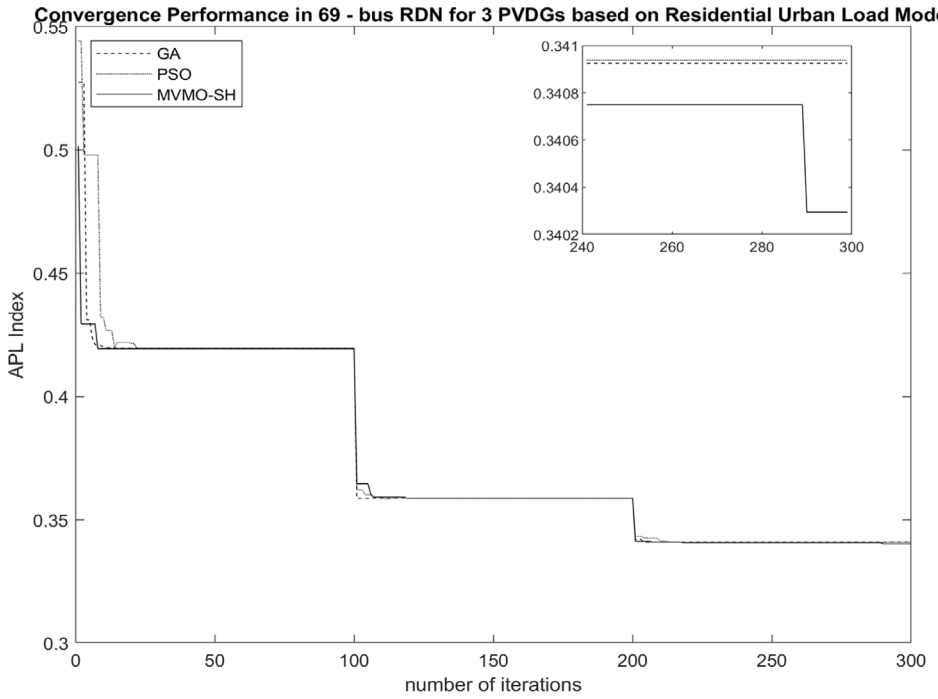

Fig. 16. Convergence performance for 3 PVDGs in 69-bus RDN based on residential urban load.

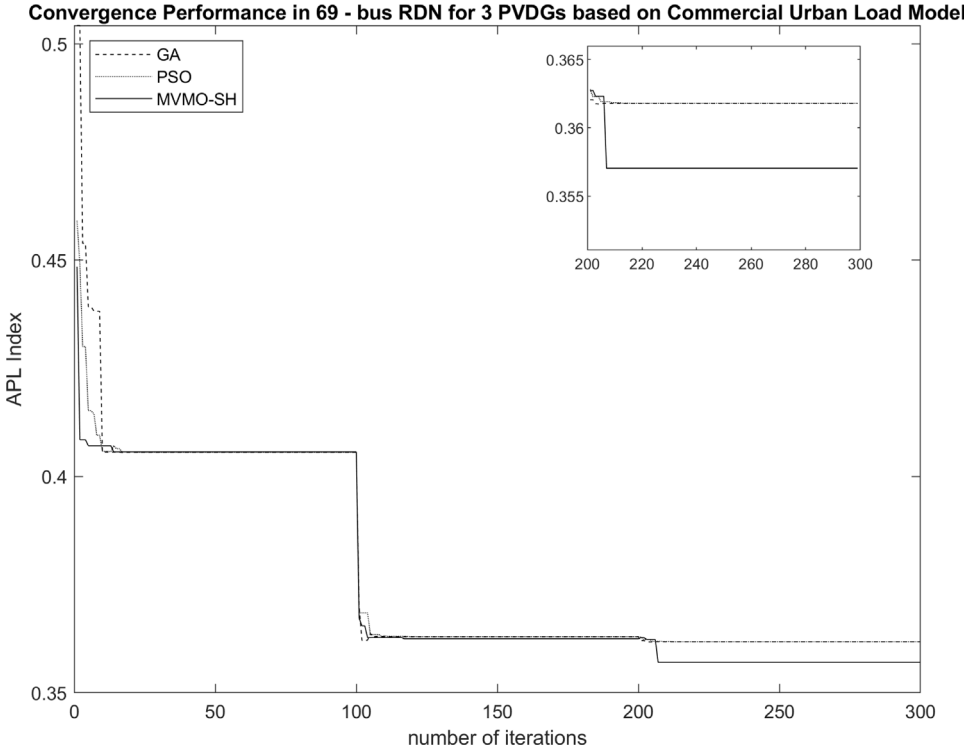

Fig. 17. Convergence performance for 3 PVDGs in 69-bus RDN based on commercial urban load.

planning of PVDG in the power system network, leading to varying PVDG locations and sizes. Compared to the results of PSO and GA, the Monte Carlo embedded MVMO-SH algorithm demonstrated better fitness evaluation performance. The proposed method showed the fastest convergence rate and lowest APL index. The MVMO-SH algorithm demonstrated superior performance, with the highest PVDG penetrations found in the industrial urban load model for the 33-bus RDN, while the commercial urban load had the highest PVDG sizes for the 69-bus RDN. The residential urban load uncertainty case showed the lowest PVDG penetrations. The significance of these findings showed that incorporating uncertainty in the optimisation framework ensures the proposed solutions become more robust and reflective of actual conditions, hence maintaining acceptable performance across various scenarios. For future directions, the energy storage system is suggested to be taken into account by considering the statistical analysis of uncertainty management in the photovoltaic generation-loads model.

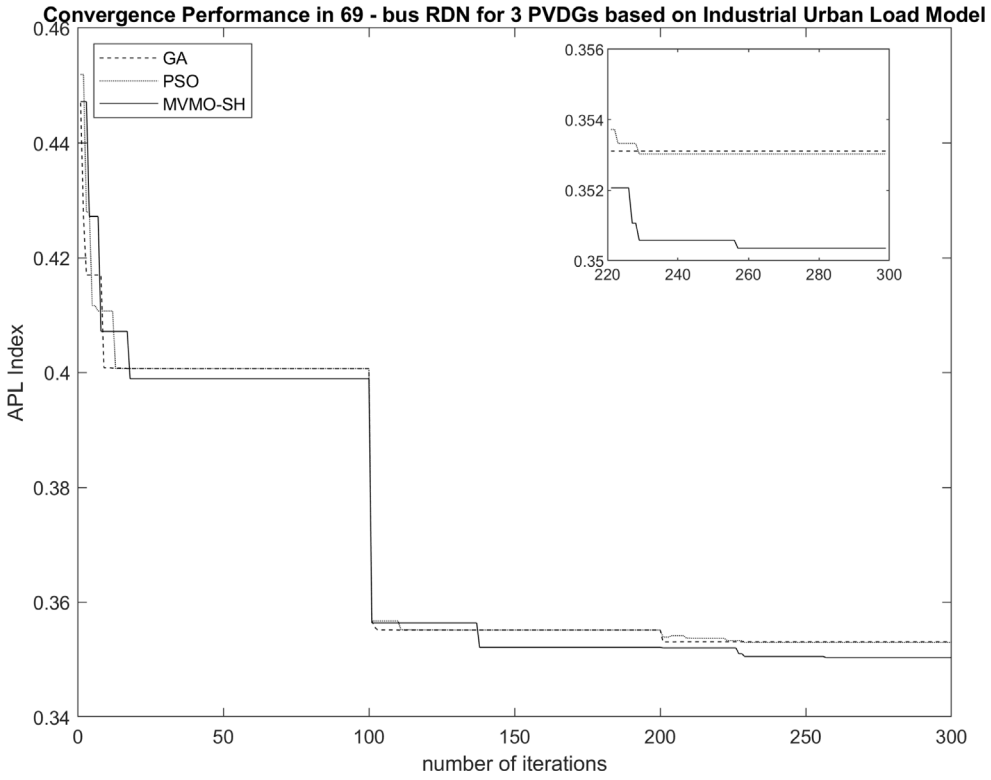

Fig. 18. Convergence performance for 3 PVDGs in 69-bus RDN based on industrial urban load.

Table 9
Statistical assessment for 3 PVDG's in 69-Bus.

Method	APL Index (Residential Urban Load Model)			
	Best Value	Worst Value	Average	Std. Deviation
MVMO-SH	0.3403	0.3587	0.3409	0.0346
PSO	0.3409	0.3588	0.3413	0.0399
GA	0.3409	0.3588	0.3411	0.0369
Method	APL Index (Commercial Urban Load Model)			
	Best Value	Worst Value	Average	Std. Deviation
MVMO-SH	0.3570	0.3625	0.3574	0.0217
PSO	0.3618	0.3629	0.3618	0.0221
GA	0.3618	0.3629	0.3618	0.0245
Method	APL Index (Industrial Urban Load Model)			
	Best Value	Worst Value	Average	Std. Deviation
MVMO-SH	0.3504	0.3521	0.3509	0.0231
PSO	0.3530	0.3552	0.3532	0.0243
GA	0.3531	0.3552	0.3531	0.0235

Declaration of competing interest

Muhamad Zahim Sujod reports financial support was provided by University Malaysia Pahang.

Data availability

Data will be made available on request.

Acknowledgements

The authors thank the Universiti Malaysia Pahang Al-Sultan Abdullah for laboratory facilities and financial support under research grant RDU210309 and RDU223001.

References

[1] N. Mlilo, J. Brown, T. Ahfock, Impact of intermittent renewable energy generation penetration on the power system networks – A review, Technol. Econ. Smart Grids Sustain. Energy 6 (1) (2021) 1–19, http://dx.doi.org/10.1007/s40866-021-00123-w.

[2] P.A. Gkaidatzis, A.S. Bouhouras, D.I. Doukas, K.I. Sgouras, D.P. Labridis, Load variations impact on optimal DG placement problem concerning energy loss reduction, Electr. Power Syst. Res. 152 (2017) 36–47.

[3] N.M. Saad others, Solar irradiance uncertainty management based on monte carlo-beta probability density function: Case in Malaysian tropical climate, Bull. Electr. Eng. Inform. 8 (3) (2019) http://dx.doi.org/10.11591/eei.v8i3.1581.

[4] M.S. Suliman, H. Hizam, M.L. Othman, Determining penetration limit of central PVDG topology considering the stochastic behaviour of PV generation and loads to reduce power losses and improve voltage profiles, IET Renew. Power Gener. 14 (14) (2020) 2629–2638, http://dx.doi.org/10.1049/iet-rpg.2019.1376.

[5] M.G. Hemeida, A.A. Ibrahim, A.A.A. Mohamed, S. Alkhalaf, A.M.B. El-Dine, Optimal allocation of distributed generators DG based manta ray foraging optimization algorithm (MRFO), Ain Shams Eng. J. 12 (1) (2021) 609–619, http://dx.doi.org/10.1016/j.asej.2020.07.009.

[6] A.S. Hassan, E.S.A. Othman, F.M. Bendary, M.A. Ebrahim, Improving the techno-economic pattern for distributed generation-based distribution networks via nature-inspired optimization algorithms, Technol. Econ. Smart Grids Sustain. Energy 7 (1) (2022) http://dx.doi.org/10.1007/s40866-022-00128-z.

[7] N. Phuangpornpitak, S. Tia, Optimal photovoltaic placement by self-organizing hierarchical binary particle swarm optimization in distribution systems, Energy Procedia 89 (2016) 69–77, http://dx.doi.org/10.1016/j.egypro.2016.05.009.

[8] H.M.H. Farh, A.M. Al-shaalan, A.M. Eltamaly, A.A. Al-shamma, A novel severity performance index for optimal allocation and sizing of photovoltaic distributed generations, Energy Rep. 6 (2020) 2180–2190, http://dx.doi.org/10.1016/j.egyr.2020.07.016.

[9] A. Jafar-nowdeh, M. Babanezhad, S. Arabi-nowdeh, Meta-heuristic matrix moth – flame algorithm for optimal reconfiguration of distribution networks and placement of solar and wind renewable sources considering reliability, Environ. Technol. Innov. 20 (101118) (2020) http://dx.doi.org/10.1016/j.eti.2020.101118.

[10] A. Eid, S. Kamel, H.M. Zawbaa, M. Dardeer, Improvement of active distribution systems with high penetration capacities of shunt reactive compensators and distributed generators using bald eagle search, Ain Shams Eng. J. 13 (6) (2022) 101792, http://dx.doi.org/10.1016/j.asej.2022.101792.

[11] N. Karmakar, B. Bhattacharyya, A reactive power planning model for power transmission systems using metaheuristics algorithms, Decis. Anal. J. 7 (February) (2023) 100224, http://dx.doi.org/10.1016/j.dajour.2023.100224.

[12] M.H. Sulaiman, Z. Mustaffa, M.I. Mohd Rashid, An application of teaching–learning-based optimization for solving the optimal power flow problem with stochastic wind and solar power generators, Results Control Optim. 10 (2022) (2023) 100187, http://dx.doi.org/10.1016/j.rico.2022.100187.

[13] R. Gupta, F. Sossan, Optimal sizing and siting of energy storage systems considering curtailable photovoltaic generation in power distribution networks, Appl. Energy 339 (2022) (2023) 120955, http://dx.doi.org/10.1016/j.apenergy.2023.120955.

[14] G.V.N. Lakshmi, A. Jayalaxmi, V. Veeramsetty, Optimal placement of distribution generation in radial distribution system using hybrid genetic dragonfly algorithm, Technol. Econ. Smart Grids Sustain. Energy 6 (1) (2021) http://dx.doi.org/10.1007/s40866-021-00107-w.

[15] A. Onlam, D. Yodphet, R. Chatthaworn, C. Surawanitkun, A. Siritaratiwat, P. Khunkitti, Power loss minimization and voltage stability improvement in electrical distribution system via network reconfiguration and distributed generation placement using novel adaptive shuffled frogs leaping algorithm, Energies 12 (553) (2019) 1–12, http://dx.doi.org/10.3390/en12030553.

[16] R. Pegado, Z. Ñaupari, Y. Molina, C. Castillo, Radial distribution network reconfiguration for power losses reduction based on improved selective BPSO, in: Electric Power Systems Research, Vol. 169, Elsevier Ltd, 2019, pp. 206–213, http://dx.doi.org/10.1016/j.epsr.2018.12.030.

[17] G. Zhang, Y. Shi, A. Maleki, M.A. Rosen, Optimal location and size of a grid-independent solar/hydrogen system for rural areas using an efficient heuristic approach, Renew. Energy 156 (2020) 1203–1214, http://dx.doi.org/10.1016/j.renene.2020.04.010.

[18] N.M. Saad others, Impacts of photovoltaic distributed generation location and size on distribution power system network, Int. J. Power Electron. Drive Syst. 9 (2) (2018) 905–913.

[19] A.A. Muhammad Al Amin Abdullah, Norhafidzah Mohd Saad, Mohammad Fadhil Abas, Norazila Jaalam, Optimization of radial distribution network with distributed generation using particle swarm optimization considering load growth, in: Proc. 6th Int. Conf. Electr. Control Comput. Eng., in: Lect. Notes Electr. Eng. - B. Ser., Springer, Singapore, 2022, pp. 257–268.

[20] A.M. Eltamaly, Y. Sayed Mohamed, A.H.M. El-Sayed, M.A. Mohamed, A. Nasr A. Elghaffar, Power quality and reliability considerations of photovoltaic distributed generation, Technol. Econ. Smart Grids Sustain. Energy 5 (1) (2020) http://dx.doi.org/10.1007/s40866-020-00096-2.

[21] A.S. Hassan, Y. Sun, Z. Wang, Multi-objective for optimal placement and sizing DG units in reducing loss of power and enhancing voltage profile using BPSO-SLFA, Energy Rep. 6 (2020) 1581–1589, http://dx.doi.org/10.1016/j.egyr.2020.06.013.

[22] E. Karunarathne, J. Pasupuleti, J. Ekanayake, D. Almeida, Optimal placement and sizing of DGs in distribution networks using MLPSO algorithm, Energies 13 (23) (2020) http://dx.doi.org/10.3390/en13236185.

[23] A. Jalili, B. Taheri, Optimal sizing and sitting of distributed generations in power distribution networks using firefly algorithm, Technol. Econ. Smart Grids Sustain. Energy 5 (1) (2020) http://dx.doi.org/10.1007/s40866-020-00081-9.

[24] Q. Zhao, S. Wang, K. Wang, B. Huang, Multi-objective optimal allocation of distributed generations under uncertainty based on D-S evidence theory and affine arithmetic, Electr. Power Energy Syst. 112 (April) (2019) 70–82.

[25] J. Radosavljevic, N. Arsic, M. Milovanovic, A. Ktena, Optimal placement and sizing of renewable distributed generation using hybrid metaheuristic algorithm, J. Mod. Power Syst. Clean Energy 8 (3) (2020) 499–510, http://dx.doi.org/10.35833/MPCE.2019.000259.

[26] J.M. Lujano-rojas, R. Dufo-lópez, J.L. Bernal-agustín, Probabilistic perspective of the optimal distributed generation integration on a distribution system, Electr. Power Syst. Res. 167 (2018) (2019) 9–20, http://dx.doi.org/10.1016/j.epsr.2018.10.015.

[27] J. Li, Optimal sizing of grid-connected photovoltaic battery systems for residential houses in Australia, Renew. Energy 136 (2019) 1245–1254, http://dx.doi.org/10.1016/j.renene.2018.09.099.

[28] G.N. Nur, C. MacKenzie, K.J. Min, A real options analysis model for generation expansion planning under uncertain demand, Decis. Anal. J. 8 (June) (2023) 100263, http://dx.doi.org/10.1016/j.dajour.2023.100263.

[29] V. Singh, T. Moger, D. Jena, Uncertainty handling techniques in power systems: A critical review, Electr. Power Syst. Res. 203 (2021) (2022) 107633, http://dx.doi.org/10.1016/j.epsr.2021.107633.

[30] M.Z. Malik, et al., Strategic planning of renewable distributed generation in radial distribution system using advanced MOPSO method, Energy Rep. 6 (November) (2020) 2872–2886, http://dx.doi.org/10.1016/j.egyr.2020.10.002.

[31] A. Arasteh, P. Alemi, M. Beiraghi, Optimal allocation of photovoltaic/ wind energy system in distribution network using meta-heuristic algorithm, Appl. Soft Comput. 109 (2021) 107594, http://dx.doi.org/10.1016/j.asoc.2021.107594.

[32] K.K. Mehmood, S.U. Khan, Z.M. Haider, C.H. Kim, A multi-agent clustering-based approach for the distributed planning of wind generators, IFAC-PapersOnLine 51 (28) (2018) 138–142, http://dx.doi.org/10.1016/j.ifacol.2018.11.691.

[33] L. Sun, et al., Determining optimal generator start-up sequence in bulk power system restoration considering uncertainties: A confidence gap decision theory based robust optimization approach, Int. J. Electr. Power Energy Syst. 153 (July) (2023) 109365, http://dx.doi.org/10.1016/j.ijepes.2023.109365.

[34] L.A. Roald, D. Pozo, A. Papavasiliou, D.K. Molzahn, J. Kazempour, A. Conejo, Power systems optimization under uncertainty: A review of methods and applications, Electr. Power Syst. Res. 214 (2023) http://dx.doi.org/10.1016/j.epsr.2022.108725.

[35] W. Wang, J. Xu, G.W. Zhang, M. Yang, X. Xu, H. Armghan, A novel chance constrained joint optimization method under uncertainties in distribution networks, Int. J. Electr. Power Energy Syst. 147 (2023) http://dx.doi.org/10.1016/j.ijepes.2022.108849.

[36] D. Huo, C. Gu, D. Greenwood, Z. Wang, P. Zhao, J. Li, Chance-constrained optimization for integrated local energy systems operation considering correlated wind generation, Int. J. Electr. Power Energy Syst. 132 (2021) http://dx.doi.org/10.1016/j.ijepes.2021.107153.

[37] J. Wang, T. Lei, X. Qi, L. Zhao, Z. Liu, Chance-constrained optimization of distributed power and heat storage in integrated energy networks, J. Energy Storage 55 (2022) http://dx.doi.org/10.1016/j.est.2022.105662.

[38] R. Xie, W. Wei, M. Li, Z. Dong, S. Mei, Sizing capacities of renewable generation, transmission, and energy storage for low-carbon power systems: A distributionally robust optimization approach, Energy 263 (2023) http://dx.doi.org/10.1016/j.energy.2022.125653.

[39] J. Radosavljević, N. Arsić, M. Milovanović, A. Ktena, Optimal placement and sizing of renewable distributed generation using hybrid metaheuristic algorithm, J. Mod. POWER Syst. Clean Energy 8 (3) (2020) 499–510, http://dx.doi.org/10.35833/MPCE.2019.000259.

[40] P.A. Gkaidatzis, A.S. Bouhouras, D.I. Doukas, Load variations impact on optimal DG placement problem concerning energy loss reduction, Electr. Power Syst. Res. 152 (November) (2017) 36–47, http://dx.doi.org/10.1016/j.epsr.2017.06.016.

[41] S.M. Arif, A. Hussain, T.T. Lie, S.M. Ahsan, H.A. Khan, Analytical hybrid particle swarm optimization algorithm for optimal siting and sizing of distributed generation in smart grid, J. Mod. Power Syst. Clean Energy 8 (6) (2020) 1221–1230, http://dx.doi.org/10.35833/MPCE.2019.000143.

[42] S. Daud, A.F.A. Kadir, C.K. Gan, A. Mohamed, T. Khatib, A comparison of heuristic optimization techniques for optimal placement and sizing of photovoltaic based distributed generation in a distribution system, Sol. Energy 140 (November) (2016) 219–226, http://dx.doi.org/10.1016/j.solener.2016.11.013.

[43] M.I. Akbar, S.A.A. Kazmi, O. Alrumayh, Z.A. Khan, A. Altamimi, M.M. Malik, A novel hybrid optimization-based algorithm for the single and multi-objective achievement with optimal DG allocations in distribution networks, IEEE Access 10 (2022) 25669–25687, http://dx.doi.org/10.1109/ACCESS.2022.3155484.

[44] M. Zeeshan, M. Kumar, A. Mahmood, Strategic planning of renewable distributed generation in radial distribution system using advanced MOPSO method, Energy Rep. 6 (October) (2020) 2872–2886, http://dx.doi.org/10.1016/j.egyr.2020.10.002.

[45] AS.Che Muhamad, N.M. Saad, M. Abas, S. Ab-Ghani, A. Ali, Optimization of Distributed Generation Using Mix-Integer Optimization by Genetic Algorithm (MIOGA) Considering Load Growth, in: Lect. Notes Electr. Eng. B. Ser. (LNEE), vol. 842, Springer Nat., 2022, pp. 245–255.

[46] J.M. Home-ortiz, M. Pourakbari-kasmaei, M. Lehtonen, J. Roberto, S. Mantovani, Optimal location–allocation of storage devices and renewable-based DG in distribution systems, Electr. Power Syst. Res. 172 (March) (2019) 11–21.

[47] M.A. Elseify, S. Kamel, H. Abdel-Mawgoud, E.E. Elattar, A novel approach based on honey badger algorithm for optimal allocation of multiple DG and capacitor in radial distribution networks considering power loss sensitivity, Mathematics 10 (12) (2022) 2081, http://dx.doi.org/10.3390/math10122081.

[48] A.A. Abdelsalam, Optimal distributed energy resources allocation for enriching reliability and economic benefits using Sine-cosine algorithm, Technol. Econ. Smart Grids Sustain. Energy 5 (1) (2020) http://dx.doi.org/10.1007/s40866-020-00082-8.

[49] W. Haider, S.J. Ul Hassan, A. Mehdi, A. Hussain, G.O.M. Adjayeng, C.H. Kim, Voltage profile enhancement and loss minimization using optimal placement and sizing of distributed generation in reconfigured network, Machines 9 (1) (2021) 1–16, http://dx.doi.org/10.3390/machines9010020.

[50] P.M. Quevedo, J. Contreras, Optimal placement of energy storage and wind power under uncertainty, Energies 9 (7) (2016) 528, http://dx.doi.org/10.3390/en9070528.

[51] S. Liu, F. Liu, T. Ding, Z. Bie, Optimal allocation of reactive power compensators and energy storages in microgrids considering uncertainty of photovoltaics, Energy Procedia 103 (April) (2016) 165–170, http://dx.doi.org/10.1016/j.egypro.2016.11.267.

[52] M. Nick, R. Cherkaoui, M. Paolone, Optimal siting and sizing of distributed energy storage systems via alternating direction method of multipliers, Int. J. Electr. Power Energy Syst. 72 (2015) 33–39, http://dx.doi.org/10.1016/j.ijepes.2015.02.008.

[53] R. Vitor, et al., Electric distribution network reconfiguration optimized for PV distributed generation and energy storage, Electr. Power Syst. Res. 184 (March) (2020) 106319, http://dx.doi.org/10.1016/j.epsr.2020.106319.

[54] M.H. Sulaiman, Z. Mustaffa, M.M. Saari, M.S. Jadin, A simulation-metaheuristic approach for finding the optimal allocation of the battery energy storage system problem in distribution networks, Decis. Anal. J. 7 (2022) (2023) 100208, http://dx.doi.org/10.1016/j.dajour.2023.100208.

[55] J. Kang, Z. Wu, T.S. Ng, B. Su, A stochastic-robust optimization model for inter-regional power system planning, European J. Oper. Res. 310 (3) (2023) 1234–1248, http://dx.doi.org/10.1016/j.ejor.2023.03.024.

[56] M.S. Shaikh, S. Raj, R. Babu, S. Kumar, K. Sagrolikar, A hybrid moth–flame algorithm with particle swarm optimization with application in power transmission and distribution, Decis. Anal. J. 6 (January) (2023) 100182, http://dx.doi.org/10.1016/j.dajour.2023.100182.

[57] S.C. Sunilkumar Agrawal, Sundaram Pandya, Pradeep Jangir, Kanak Kalita, A multi-objective thermal exchange optimisation model for solving optimal power flow problems in hybrid power systems, Decis. Anal. J. (2023) (2023) 100299, http://dx.doi.org/10.1016/j.dajour.2023.100299.

[58] X. Zong, Y. Yuan, Two-stage robust optimization of regional integrated energy systems considering uncertainties of distributed energy stations, Front. Energy Res. 11 (March) (2023) 1–16, http://dx.doi.org/10.3389/fenrg.2023.1135056.

[59] R.O. Bawazir, N.S. Cetin, Comprehensive overview of optimizing PV-DG allocation in power system and solar energy resource potential assessments, Energy Rep. 6 (January) (2020) 173–208, http://dx.doi.org/10.1016/j.egyr.2019.12.010.

[60] J.L. Rueda, I. Erlich, MVMO for bound constrained single-objective computationally expensive numerical optimization, in: IEEE Congress on Evolutionary Computation, (CEC), 2015, pp. 1011–1017.

[61] W. Nakawiro, I. Erlich, J.L. Rueda, A novel optimization algorithm for optimal reactive power dispatch: A comparative study, in: 4th International Conference on Electric Utility Deregulation and Restructuring and Power Technologies (DRPT), (1), 2011, pp. 1555–1561, http://dx.doi.org/10.1109/DRPT.2011.5994144.

[62] I. Erlich, B. Sager, Optimal allocation and sizing of capacitor banks for maximum power transfer to selected areas, 2017.

[63] J.L. Rueda, W.H. Guamán, J.C. Cepeda, I. Erlich, A. Vargas, Hybrid approach for power system operational planning with smart grid and small-signal stability enhancement considerations, IEEE Trans. Smart Grid 4 (1) (2013) 530–539, http://dx.doi.org/10.1109/TSG.2012.2222678.

[64] José L. Rueda, István Erlich, Optimal dispatch of reactive power sources by using MVMO s optimization, in: IEEE Symposium on Computational Intelligence Applications in Smart Grid (CIASG), 0, (1), 2013, pp. 29–36.

[65] J. Kennedy, R. Eberhart, Particle swarm optimization, in: IEEE International Conference on Neural Networks, 1995, pp. 1942–1948, http://dx.doi.org/10.1007/978-3-319-46173-1_2.

[66] N.M. Saad, M.Z. Sujod, M.I.M. Ridzuan, M.F. Abas, Optimization for distributed generation planning in radial distribution network using MVMO-SH, 2019, http://dx.doi.org/10.1109/ICSGRC.2019.8837082.

[67] M.H. Moradi, M. Abedini, A novel method for optimal DG units capacity and location in microgrids, Int. J. Electr. Power Energy Syst. 75 (2016) 236–244, http://dx.doi.org/10.1016/j.ijepes.2015.09.013.